Energy & Environmental Science

PERSPECTIVE

View Article Online
View Journal | View Issue

Applications of functional fullerene materials in polymer solar cells

Cite this: *Energy Environ. Sci.*, 2014, **7**, 1866

Yu-Ying Lai, Yen-Ju Cheng* and Chain-Shu Hsu*

Bulk heterojunction (BHJ) polymer solar cells (PSCs) on the basis of polymer:fullerene blends have delivered numerous impressive results in the last decade and thus have drawn much attention of the scientific and industrial communities. However, BHJ PSCs often suffer from several intrinsic problems, such as the low open-circuit voltage (V_{oc}), energetically-unfavorable and chemically-incompatible interfaces, and morphological phase separation of the polymer:fullerene blend driven by thermal treatment, hindering further advancement. In this review, we summarize the recent progress on applications of fullerene-based materials in the BHJ PSCs. Bis-adduct fullerenes possessing high-lying LUMO energy levels can substitute for mono-substituted fullerenes and higher V_{oc} values can thus be achieved. Incorporation of an n-type fullerene interlayer between inorganic and organic active layers in either inverted or conventional PSCs can help in minimization of charge recombination losses at the interface and improvement of charge transfer from the active layer to the inorganic layer, thus resulting in superior PCEs. The optimal active-layer morphology can be maintained through several approaches, such as *in situ* polymerization of cross-linkable fullerenes, suppression of large-scale $PC_{61}BM$ aggregation by a polyethylene glycol-functionalized fullerene, supramolecular pentafluorophenyl-fullerene stabilization, and light-induced oligomerization of fullerenes. The morphological phase separation of the active-layer materials can thus be minimized. The research of employing fullerene materials will continue playing a critical role in BHJ PSCs. With further investigation and advancement in this field, it is expected that the ultimate goal of commercialization can be realized.

Received 12th September 2013
Accepted 6th February 2014

DOI: 10.1039/c3ee43080d

www.rsc.org/ees

Broader context

Since bulk heterojunction solar cells were developed in 1995, fullerene derivatives have been dominating in n-type materials due to their low-lying lowest unoccupied molecular orbital (LUMO) energy levels, fast photo-induced electron-transfer and high intrinsic electron mobility. The intrinsic molecular properties of fullerene materials can be custom-tailored by covalently incorporation of functional groups on the buckyballs. The electronic and steric effects exerted by the attached adducts could be used to modulate the optical properties, frontier orbitals, intermolecular interaction, and recrystallization of the fullerenes. Double functionalization of fullerenes has been an effective strategy to arise the LUMO energy levels with greater V_{oc} values of the devices. With the aid of the functional groups to ensure solution processability, the fullerene materials can also act as an electron-selective buffer layer in either regular or inverted devices. More importantly, the functional groups can form chemical interaction/bonding with the metal oxides or electrodes to strengthen interfacial characteristics and facilitate electron-transportation, leading to the improvement of the device performance. Through covalent cross-linking or noncovalent interactions to suppress the aggregation of fullerenes, the optimized morphology of active layers can be permanently preserved against long-term thermal heating. The incorporation of well-designed functional groups has provided fullerene derivatives with versatile functions to achieve highly efficient and stable solar cells.

1. Introduction

Research on polymer solar cells (PSCs) consisting of organic p-type polymer (donor) and n-type fullerene (acceptor) semiconductors has attracted tremendous scientific and industrial interest in recent years.[1,2] The general working principle for PSCs first involves photoexcitation of the donor material by absorption of light energy to generate excitons. This Coulomb-correlated electron–hole pair diffuses to the donor–acceptor (D–A) interface, where exciton dissociation occurs. Since the limited lifetime scale only allows excitons to diffuse a short distance (5–14 nm),[3–8] donor excitons created remote from the heterojunction interface decay to the ground state before they reach the D–A interfaces, leading to the loss of absorbed photons and quantum efficiency. In order to increase the D–A interfacial area for efficient charge separation, bulk heterojunction (BHJ) is thus adopted to establish an interpenetrating network of donor and acceptor materials.[1,2]

A conventional BHJ PSC with an active layer sandwiched by a low-work-function aluminum cathode and a hole-conducting

Department of Applied Chemistry, National Chiao Tung University, 1001 Ta Hseuh Road, Hsin-Chu, 30010 Taiwan. E-mail: yjcheng@mail.nctu.edu.tw; cshsu@mail.nctu.edu.tw

poly(3,4-ethylenedioxythiophene):poly(4-styrenesulfonic acid) (PEDOT:PSS) layer on top of an indium tin oxide (ITO) substrate is the most widely used and investigated device configuration. The combination of poly(3-hexylthiophene) (P3HT) as electron donor and [6,6]-phenyl-C_{61} butyric acid methyl ester ($PC_{61}BM$) as electron acceptor in the active layer represents one of the most efficient BHJ solar cells with power conversion efficiencies (PCEs) approaching 5%.[9–13] However, in order to achieve the ultimate goal of commercialization, further optimization is utterly required. To begin with, we will describe the most critical difficulties encountered in the research of the PSCs and discuss the potential solutions towards these challenges.

1.1 Low open-circuit voltage (V_{oc})

One of the most noticeable restrictions for numerous polymer:fullerene-based devices is the low open-circuit voltage (V_{oc}), limiting further advancement of device performance. It has been demonstrated that the magnitude of V_{oc} value shows a linear relationship with the energy difference between the highest occupied molecular orbital (HOMO) energy level of polymers and the lowest unoccupied molecular orbital (LUMO) level of fullerenes.[14–16] From the perspective of adjusting molecular energy level, either lowering the HOMO energy level of the p-type polymer (donor) or raising the LUMO energy level of the n-type fullerene (acceptor) could in principle reach larger V_{oc} values. Given that fullerene derivatives have been regarded as irreplaceable n-type materials for high-performance BHJ solar cells, developing new fullerene-based materials that possess intrinsically high-lying LUMO energy levels would be a more practicable alternative to optimize the V_{oc} value.

1.2 Energetically unfavorable and chemically-incompatible interfaces

Along with high performance, long-term stability is another primary area of concern for PSCs. Rapid oxidation of the low-work-function Al cathode and etching of ITO by the acidic PEDOT:PSS layer are the most common causes of instability in conventional unencapsulated solar devices. An effective approach to solving these problems and improving the device lifetime is to fabricate inverted PSCs.[17–20] By reversing the polarity of charge collection in a regular cell, air-stable Ag combining with an adjacent hole-transporting layer, such as PEDOT:PSS or MoO_3, can substitute for air-sensitive Al as the anodic electrode for efficient hole collection. In such an inverted configuration, it is often required to insert inorganic metal oxide (TiO_x or ZnO) between ITO and the active layer to function as an electron-selective contact.[21–25] However, the energetical unfavorability and chemical incompatibility existing in interfaces may lead to the depreciation of device performance.[26] For instance, surface hydroxyl groups on metal oxide are known to

Yu-Ying Lai received his diploma and Master degree in Chemistry from National Taiwan Normal University and National Taiwan University, respectively. He obtained his PhD degree from the department of chemistry and applied biosciences at ETH Zürich, Switzerland under the supervision of Prof. Peter Chen. Afterwards, he joined Prof. Yen-Ju Cheng's group in National Chiao-Tung University as a Postdoctoral fellow. His research interest focuses on the use of experimental and computational approaches to improve the organic-solar-cell technology.

Yen-Ju Cheng received his PhD degree in chemistry from the National Taiwan University in 2004 under supervision of Prof. Tien-Yau Luh. After spending another year as a postdoc with Prof. Luh at NTU, he joined Prof. Alex K.-Y. Jen's group as a post-doctoral researcher at the University of Washington in 2005. In the summer of 2008, he joined the Department of Applied Chemistry, National Chiao Tung University in Taiwan as an assistant professor and was promoted to associate professor in 2011. His current research interest is focused on the design, synthesis and characterization of organic and polymeric functional materials for optoelectronic and photovoltaic applications.

Chain-Shu Hsu received his Ph.D. degree from Case Western Reserve University in 1987 and conducted his postdoctoral work at National Tsing Hua University in Taiwan. He joined the Department of Applied Chemistry of the National Chiao Tung University, Taiwan in 1988 as an associate professor and was promoted to full professor in 1991. Currently he is serving as a vice president and chair professor of the National Chiao Tung University. His research interests include liquid crystalline polymers and conjugated polymers, polymer light-emitting diodes, and organic photovoltaics. He received the Excellent Research Award of National Science Council, Taiwan in 1994, the Franco-Taiwan Scientific Award on nanomaterials in 2006, the Teco and Hou Chin Tui Awards in 2007, and the Academic Award of the Ministry of Education, Taiwan in 2008.

act as electron traps, being harmful to the charge transport at the interface between the metal oxide and the organic layer.[27–29] Interfacial modification by incorporating an additional n-type fullerene interconnection layer between the inorganic metal oxide and the organic active layer can provide a practical solution for improving the inverted device performance by modulating the electronic and orbital interactions at the upper and lower interfaces.[30] Moreover, it can also be applied to the conventional configuration. The improvement of device characteristics can be achieved by installation of a fullerene-based interconnection layer between the active layer and the cathode, being expected to increase the charge-transporting efficiency.[31–33]

1.3 Morphology evolution

Prudently controlling the phase separation between two components in the bulk to reach ideal D–A morphology plays an significant role in the success of various polymer:fullerene systems. For example, thermal annealing of a P3HT:$PC_{61}BM$ composite drives P3HT to reorganize and self assemble, resulting in the enhancement of crystallinity of P3HT. Through this morphological evolution, a featureless and homogeneous blend gradually reaches a bicontinuous interpenetrating D–A network with optimal D–A domain size.[9] Accordingly, maximal D–A interfacial area for efficient charge separation and optimal D–A arrangement for superior charge transportation can be achieved.[34] Unfortunately, this optimal morphology is a kinetically trapped intermediate which readily moves toward a more thermodynamically stable state if thermal annealing at elevated temperatures is applied constantly.[35–40] As illustrated in Fig. 1, the P3HT domain continues to undergo further crystallization, while the spherical $PC_{61}BM$, with its high molecular mobility, tends to diffuse out of the polymer matrix and aggregate into larger clusters.[38,39,41] Such progressive phase segregation between P3HT and $PC_{61}BM$ eventually leads to the reduction of the percolating electron transport pathways within the mixed regions and thus adversely augments charge recombination losses. Generally speaking, given that a photovoltaic device must be exposed to long-term sunlight irradiation, the accumulated heat generated by long-term sunlight irradiation may destroy the optimal D–A morphology and deteriorate the device performance.[42] To reduce the crystallinity of polymers[43] or fullerene derivatives[44,45] can help in maintaining the active-layer morphology. However, from the perspective of general applicability, stabilizing the optimal D–A morphology by introducing a compatibilizer to impart secondary interactions between donor and acceptor constituents or *in situ* chemical cross-linking between components in active layers are a more straightforward strategy. In comparison to the plentiful p-type materials, n-type materials are still dominated by fullerene-based derivatives. Therefore, incorporation of compatibilizer or cross linker moieties into fullerene-based materials is considered to be a feasible approach to stabilize the active-layer morphology.

In view of the great potential and applicability of the fullerene derivatives in the further improvement of the BHJ device performance and long-term stability, we review the recent research progress on applications of fullerene-based materials in the BHJ PSCs. The discussion will be focused on three topics: bis-adduct fullerenes, fullerene-based interlayer modification, and morphological stabilization. It should be noted that the synthetic complexity and efficiency are important issues for commercialization. The synthetic approaches for most fullerene materials mentioned in the following sections are rather easy and straightforward, which is advantageous to the ultimate goal of commercialization.

2. Bis-adduct fullerenes

Incorporation of electron-donating groups (EDGs) on the peripheral side of pristine C_{60} has been utilized to elevate the LUMO energy level of fullerenes.[44,46,47] However, owing to no direct conjugation between the EDG and the core C_{60}, the through-space electronic effect is relatively weak. Therefore, the variations in the LUMO energy level of fullerene derivatives are not significant enough to affect the V_{oc}. Recently, bis-adduct C_{60} derivatives have emerged as new materials with higher-lying LUMO energy levels than their corresponding mono-adduct C_{60} analogues.[48–52] The second functionalization on the core structure of the mono-substituted C_{60} further reduces the π-conjugation and electron delocalization in the C_{60}. The formed bis-adduct C_{60} derivatives can in principle have larger

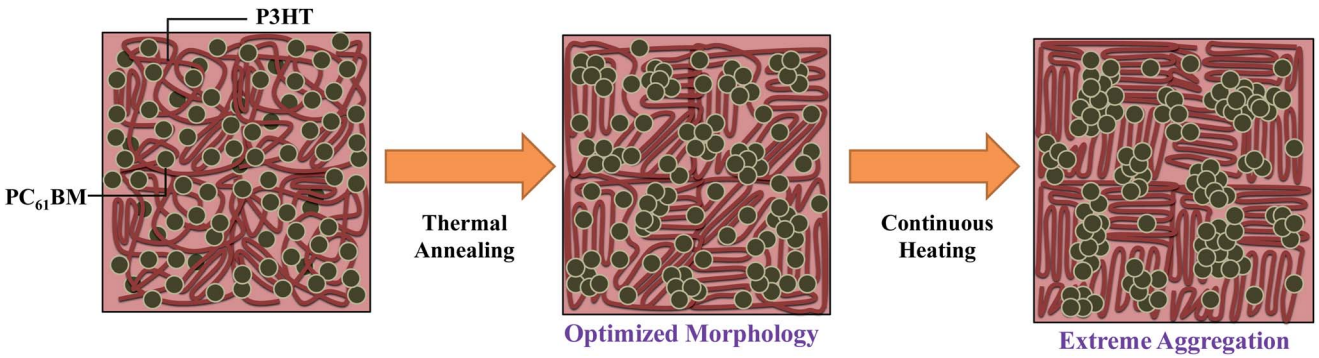

Fig. 1 Morphological evolution of the P3HT:$PC_{61}BM$ blend under thermal treatment. Reprinted with permission from ref. 129. Copyright 2013, Wiley-VCH Verlag GmbH & Co. KGaA.

electrochemical reduction potentials and thus higher-lying LUMO levels.

2.1 BisPCBM

BisPCBM is the bis-adduct analogue of $PC_{61}BM$ (Scheme 1). The LUMO level of bisPCBM is *ca.* 100 mV higher than that of $PC_{61}BM$. Owing to its structural similarity to $PC_{61}BM$, bisPCBM was tested in conventional PSC devices.[48] A device on the basis of ITO/PEDOT:PSS/P3HT:bisPCBM (1 : 1.2, w/w)/Sm/Al configuration gave a PCE of 4.5% (Entry 1, Table 1). This PCE value is about a factor of 1.2 larger than that of the reference P3HT:$PC_{61}BM$ cell (3.8%).[48] As expected, this improvement is mainly due to the increase of the V_{oc} value.

2.2 ICBA, $IC_{70}BA$, and IPCBM

Subsequent to the development of bisPCBM, Li and co-workers designed and synthesized another C_{60} bis-adduct, ICBA (Scheme 1).[49] The LUMO level of ICBA is raised by 0.17 eV and 0.07 eV, respectively, in comparison to that of $PC_{61}BM$ and bisPCBM. The PCE value for the P3HT:ICBA blend was initially determined to be 5.44% based on the ITO/PEDOT:PSS/P3HT:ICBA (1 : 1, w/w)/Ca/Al configuration (Entry 2, Table 1). By solvent and thermal annealing of the P3HT:ICBA blend, the PCE value was further improved to 6.48% (Entry 3, Table 1).[51] Again, in comparison to the P3HT:$PC_{61}BM$ reference cell (Entry 4, Table 1),[49] the improvement in PCE mainly comes from the significant increment in V_{oc}.

It is acknowledged that C_{60} derivatives have weak visible-light absorption than their C_{70} analogues. An indene-C_{70} bis-adduct $IC_{70}BA$ (Scheme 1) was thus developed in order to enhance the absorption ability of the active layer.[53] As expected, $IC_{70}BA$ has enhanced visible-light absorption and its LUMO energy level is *ca.* 0.19 V higher than that of $PC_{61}BM$. Initially, a device based on P3HT:$IC_{70}BA$ furnished a high V_{oc} of 0.84 V and a PCE of 5.64% (Entry 5, Table 1).[53] Further device optimization resulted in a PCE of 6.69% (Entry 6, Table 1) with 3-methylthiophene as a processing additive[54] and 6.68% (Entry 7, Table 1) with MoO_3 to replace PEDOT:PSS as an anode buffer layer.[55] More importantly, when 1-chloronaphthalene was adopted to be the processing additive for the P3HT:$IC_{70}BA$ blend, an impressive PCE of 7.40% (Entry 8, Table 1) was obtained.[56]

A $PC_{61}BM$ derivative, indene-PCBM (IPCBM, Scheme 1) was also developed.[57] It is highly soluble in common organic solvents and its LUMO energy level is 0.12 eV higher than that of $PC_{61}BM$. In comparison to ICBA and $IC_{70}BA$, the slightly lower LUMO energy level of IPCBM is beneficial for charge separation from donor to acceptor, especially for small bandgap polymers. A device based on P3HT:IPCBM delivered a V_{oc} of 0.72 V and a PCE of 4.39% (Entry 9, Table 1).[57] By installing an electron transportation layer of PFCn6:K^+ (Scheme 1) between the active layer and the cathode, the PCE was further improved to 6.63% with a V_{oc} of 0.86 V, a J_{sc} of 10.93 mA cm^{-2}, and an FF of 70.6% (Entry 10, Table 1).[58]

2.3 Bis-TOQC

A thieno-*o*-quinodimethane functionalized C_{60} bisadduct (bis-TOQC, Scheme 1) also shows potential in enhancing the PSC performance.[59] A conventional device based on the ITO/PEDOT:PSS/P3HT:bis-TOQC (1 : 0.6, w/w)/Ca/Al configuration delivered a good PCE of 5.1% under simulated 86 mW cm^{-2} AM 1.5G illumination (Entry 11, Table 1). Compared to a P3HT:$PC_{61}BM$-based regular device, the performance enhancement mainly comes from the increment of the V_{oc} value that is directly linked to the high LUMO energy level of bis-TOQC. It should be noted that the attempt to install solubilizing groups at the 5-position of thiophene of bis-TOQC degraded the

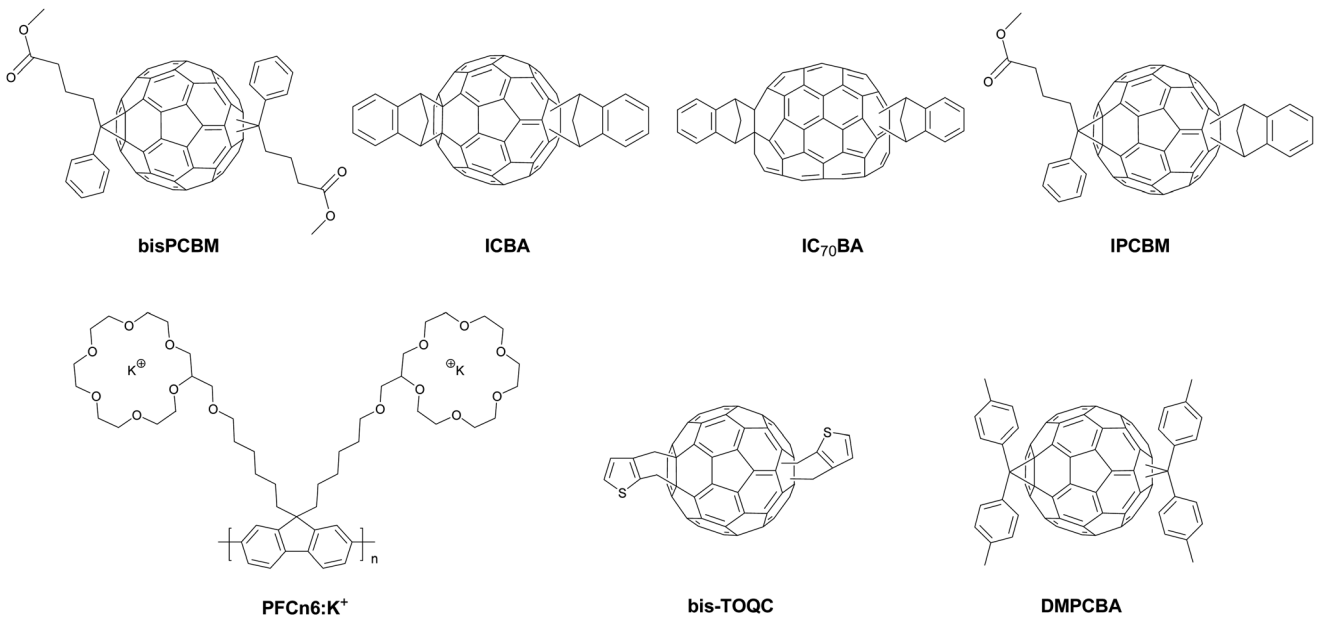

Scheme 1 Structures of bisPCBM, ICBA, $IC_{70}BA$, IPCBM, PFCn6:K^+, bis-TOQC, and DMPCBA.

Table 1 Device characteristics of the P3HT-based PSCs with different acceptors

Entry	Active layer	Weight ratio (in wt%)	V_{oc} (V)	J_{sc} (mA cm^{-2})	FF (%)	PCE (%)	Electron mobility (cm^2 V^{-1} s^{-1})
1	P3HT/bisPCBM[a,48]	1 : 1.2	0.72	9.14	68.0	4.50	7.0×10^{-4}
2	P3HT/ICBA[b,49]	1 : 1	0.84	9.67	67.0	5.44	N/A[h]
3	P3HT/ICBA[b,c,51]	1 : 1	0.84	10.61	72.7	6.48	N/A
4	P3HT/$PC_{61}BM$[b,49]	1 : 1	0.58	10.8	62.0	3.88	N/A
5	P3HT/$IC_{70}BA$[b,53]	1 : 1	0.84	9.73	69.0	5.64	N/A
6	P3HT/$IC_{70}BA$[b,e,54]	1 : 1	0.86	10.79	72.1	6.69	N/A
7	P3HT/$IC_{70}BA$[d,55]	1 : 1	0.85	10.61	74.1	6.68	N/A
8	P3HT/$IC_{70}BA$[b,f,56]	1 : 1	0.87	11.35	75.0	7.40	N/A
9	P3HT/IPCBM[b,57]	1 : 1.5	0.72	9.49	64.0	4.39	N/A
10	P3HT/IPCBM[g,58]	1 : 1	0.86	10.93	70.6	6.63	N/A
11	P3HT/bis-TOQC[b,j,59]	1 : 0.6	0.86	7.70	66.0	5.10	N/A
12	P3HT/DMPCBA[b,61]	1 : 1.2	0.87	9.05	65.5	5.20	9.0×10^{-5}[i]
13	P3HT/$PC_{61}BM$[b,61]	1 : 1	0.60	9.65	67.4	3.90	1.3×10^{-4}[i]

[a] ITO/PEDOT:PSS/P3HT:bisPCBM/Sm/Al. [b] ITO/PEDOT:PSS/P3HT:acceptor/Ca/Al. [c] Thermal annealing of the active layer at 150 °C for 10 min. [d] ITO/MoO_3/P3HT:acceptor/Ca/Al. [e] With 3 vol% 3-methylthiophene as the processing additive. [f] With 3 vol% 1-chloronaphthalene as the processing additive. [g] ITO/PEDOT:PSS/P3HT:acceptor/PFCn6:K^+/Ca/Al. [h] N/A = not available. [i] Based on ITO/Al/P3HT:acceptor/Ca/Al device by using SCLC theory. [j] Device parameters were characterized under simulated 86 mW cm^{-2} AM 1.5G illumination.

device efficiency significantly. The presence of aliphatic side chains may hamper the intermolecular stacking between fullerenes and thus result in inferior electron transport ability, bringing negative effect on the PSC performance.[60]

2.4 DMPCBA

The function of bis-adduct fullerenes is not merely limited in the increment of V_{oc}. We recently developed a di(4-methylphenyl)methano-C_{60} bis-adduct, DMPCBA (Scheme 1).[61] Similar to other bis-adduct fullerenes, DMPCBA has a higher LUMO energy level by *ca.* 100 mV over $PC_{61}BM$. Noticeably, differential scanning calorimetry (DSC) measurements revealed that DMPCBA doesn't exhibit melting thermal transition, while a sharp melting point at 280 °C was detected for $PC_{61}BM$. The absence of the melting transition for DMPCBA indicates that it is an amorphous glass that has no tendency toward thermal-driven crystallization. Wudl and co-workers have demonstrated that the planes of the two phenyl rings in diphenylmethanofullerene prefer to lie parallel to the fullerene surface.[62] Therefore, the geometry of the two germinal diphenyl groups in DMPCBA can sterically protect and shield the core C_{60} structure from severe intermolecular aggregation, rendering it intrinsically amorphous and highly soluble. It can thus be anticipated that progressive phase segregation to micrometer-sized D–A domains may thus be alleviated with DMPCBA as the donor material in the active layer.

The possibility of employing DMPCBA in BHJ solar devices was then examined.[61] A conventional device based on ITO/PEDOT:PSS/P3HT:DMPCBA (1 : 1.2, w/w)/Ca/Al exhibited a V_{oc} of 0.87 V, a J_{sc} of 9.05 mA cm^{-2}, and a high FF of 65.5%, yielding a high PCE of 5.2% (Entry 12, Table 1). Yet again, the improved PCE in the P3HT:DMPCBA cell to that of the P3HT:$PC_{61}BM$ reference device (Entry 13, Table 1) mainly results from the significant enlargement of V_{oc}. Furthermore, the morphological stability was also tested. The devices were isothermally heated at 160 °C for 10 and 20 h prior to the deposition of the top electrode. The efficiency of the P3HT:$PC_{61}BM$ reference device decreased dramatically, from 3.9% to 0.7% after 20 h of isothermal heating. In sharp contrast, the DMPCBA-based cell exhibited much more stable device characteristics and the PCE smoothly degraded to 4.7% after 10 h of heating and to 4.2% over 20 h of heating. Optical microscopy revealed that thermal annealing of the P3HT:$PC_{61}BM$ blend induced a severe macrographic alteration, forming needle-shaped $PC_{61}BM$ crystals hundreds of micrometers in length.[63–65] Nevertheless, the morphology of the P3HT:DMPCBA (1 : 1.2, w/w) blend remains almost unchanged before and after the thermal annealing. The high thermal stability is ascribed to the amorphous nature of DMPCBA that preserves the device characteristics.

3. Fullerene-based interlayer modification

Hashimoto and co-workers have demonstrated that self-organization of a fluorinated $PC_{61}BM$ buffer layer on top of a P3HT:$PC_{61}BM$ active layer is able to improve the photovoltaic performance of a regular PSC.[30] Moreover, Jen and co-workers have synthesized a series of C_{60} derivatives having acid or alcohol groups, which can form a self-assembled monolayer (SAM) on the TiO_x or ZnO surface in an inverted PSC and the corresponding device efficiency was then improved.[66–68] Subsequently, much research effort has evolved in the area of interfacial modification by incorporating an additional n-type fullerene interlayer between inorganic and organic active layers. In this section, we will discuss the recent development on the fullerene-based interfacial modification in regular as well as inverted devices. The discussions are classified according to the functional groups covalently attached to the fullerenes. Generally speaking, the capabilities of these fullerenes can be sorted into two categories: one is to enhance the interfacial charge-

transport efficiency and the other is to modify the work function of cathodes.

3.1 Acid and alcohol groups

It was found that the C_{60}-SAMs with various anchoring groups, *i.e.*, carboxylic acid (C_{60}-acid, PCBM-acid, and C_{60}-acid_2), phosphonic acid (C_{60}-PA), and catechol (C_{60}-catechol), can be formed onto the surface of ZnO or TiO_x by simple solution-based process (Scheme 2).[66–68] For instance, inverted P3HT:PC_{61}BM-based BHJ solar cells with intercalation of the C_{60}-acid or C_{60}-catechol SAM between the active layer and ZnO were fabricated. Under optimized SAM assembly conditions, the device efficiency improved from 3.47 (without C_{60}SAM) to *ca.* 4.4% (with C_{60}-acid) and 4.19% (with C_{60}-catechol) (Entry 1–3, Table 2).[68] The PCE improvement when modified with a C_{60}-SAM is mainly attributed to the enhancement of J_{sc} and FF (Entry 1–3, Table 2). The C_{60}-SAM interlayer acts as an electron selective and hole blocking layer, and its presence can help in minimization of charge recombination losses at the interface owing to the improved charge transfer from the active layer to the ZnO layer. The larger photocurrent can thus be achieved.

Not merely limited in inverted solar devices, acid or alcohol functionalized fullerenes can also be utilized in conventional devices. Nevertheless, potential difficulties derived from solution processing of the fullerene-based interlayer need be taken into account. Active-layer organic materials, *e.g.*, P3HT:PC_{61}BM, are usually soluble in common organic solvents. Organic solvents that dissolve the active-layer materials must be avoided when incorporating the fullerene-based interlayer on top of the active layer in the regular devices. Otherwise, severe intermixing between the two layers may occur, leading to the structural deterioration of the active layer. Accordingly, we developed two hydrophilic fullerene derivatives, bis(triethylene glycol) malonate C_{60} (EGMC-OH) and bis(triethylene glycol phthalic acid)-malonate C_{60} (EGMC-COOH), with hydroxyl and acid groups as the outmost moieties respectively (Scheme 2).[69] With the aid of triethylene glycol-based side chains, these C_{60} materials with enhanced hydrophilic nature can be dissolved in the polar 2-ethoxyethanol/H_2O solvent and then spin-cast to form an interlayer without destroying the underneath active layer. BHJ solar devices on the basis of ITO/PEDOT:PSS/P3HT:PC_{61}BM/interlayer/Ca/Al were then fabricated. The power conversion efficiency (PCE) was increased from 3.61% to 3.71% and 3.80% by using EGMC-OH and EGMC-COOH as the electron-selective modification layer (EML) materials, respectively (Entry 4–6, Table 2). Moreover, the electron transporting properties of EGMC-OH and EGMC-COOH can be further enhanced by the incorporation of alkali carbonates as the n-dopants. Regardless of the counter ions, Cs_2CO_3, Li_2CO_3, as well as K_2CO_3 are all effective in obtaining high PCEs. The device using EGMC-COOH doped with 40 wt% Li_2CO_3 achieved a highest PCE of 4.29% (Entry 7, Table 2). The alcohol/water soluble EGMC-COOH is applicable to other conventional devices as well. With the incorporation of the EGMC-COOH EML doped with 40 wt% Li_2CO_3, the PCDCTBT-C8 (Scheme 2):PC_{71}BM-based device exhibited a superior PCE of 4.51%, which outperformed the corresponding non-modified device with a PCE of 3.63% (Entry 8–9, Table 2).

3.2 Phosphoric ester groups

An alcohol soluble fullerene material, B-PCPO (Scheme 2) was developed and used in PSCs owing to the fact that it has the properties of good alcohol processability, ITO modification function, and good electron transporting ability.[70] An inverted device in the absence of EML by using the ITO/PCDTBT (Scheme 2):PC_{71}BM/MoO_3/Al configuration gave a PCE value of 4.83% with a V_{oc} of 0.71 V, a J_{sc} of 10.20 mA cm^{-2}, and an FF of 56.1% (Entry 10, Table 2). By using B-PCPO as the EML between ITO and the active layer (PCDTBT:PC_{71}BM), the corresponding device delivered a high PCE of 6.20% with a V_{oc} of 0.89 V, a J_{sc} of 9.50 mA cm^{-2}, and an FF of 61.7% (Entry 11, Table 2). As listed in Table 2, with the assistance of B-PCPO, V_{oc} and FF were both enhanced, leading to a higher overall performance, even though J_{sc} was slightly decreased. X-ray photoelectron spectroscopy (XPS) revealed that the work function of ITO is decreased by ~0.4 eV by introduction of a thin B-PCPO layer, which may result from the dipole formation in the ITO/active layer interface.[71,72] The lower work function of ITO is beneficial for increasing the built-in potential of PSCs, in turn leading to the enhanced V_{oc}.[73,74] Moreover, the decrease of ITO work function can also offer better energy level alignment with the LUMO level of PC_{71}BM and thereby facilitate the electron transporting and collection, transforming to the enhancement of FF.

3.3 Polyethylene glycol groups

High work function metals, such as Ag, have been used as cathodes to substitute for Al in conventional PSCs on account of their high stability to ambient conditions. However, the high work function often results in low V_{oc} and poor device performance.[74–76] Two polyethylene glycol (PEG)-based fullerene surfactants, ETL-1 and ETL-2 (Scheme 2), were found to be effective in tuning the work function of metal cathode and also increasing the photocurrent generation when used as an interfacial layer between the active layer and the metal cathode.[77,78] Besides, the presence of PEG renders these two compounds highly soluble in alcoholic solvents, which is good for utilizing orthogonal solvent-processed strategies.[79,80] ETL-1 and ETL-2 with the cationic tetrahydro pyrrole and PEG addend can up-shift the work function of Ag by 0.8 eV.[78] The device configuration of ITO/PEDOT:PSS/PIDT-PhanQ (Scheme 2):PC_{71}BM/interlayer/Ag was tested. In comparison to the reference cell without interlayer (Entry 12, Table 2), significant improvement of PCE was observed for devices with installation of ETL-1 or ETL-2 between the active layer and the Ag cathode (Entry 13–14, Table 2). The presence of ETL-1 or ETL-2 can simultaneously improve V_{oc}, J_{sc}, and FF, thus resulting in high-performance PSCs using the high work-function Ag cathode.

Calcium is known to be highly reactive to moisture and thermal evaporation under vacuum is an inevitable step for processing Ca in solar devices. A solution processable PEG-modified C_{60} (PEGN-C_{60}, Scheme 2) was thus proposed to replace Ca in conventional solar devices.[81] It was tested under the

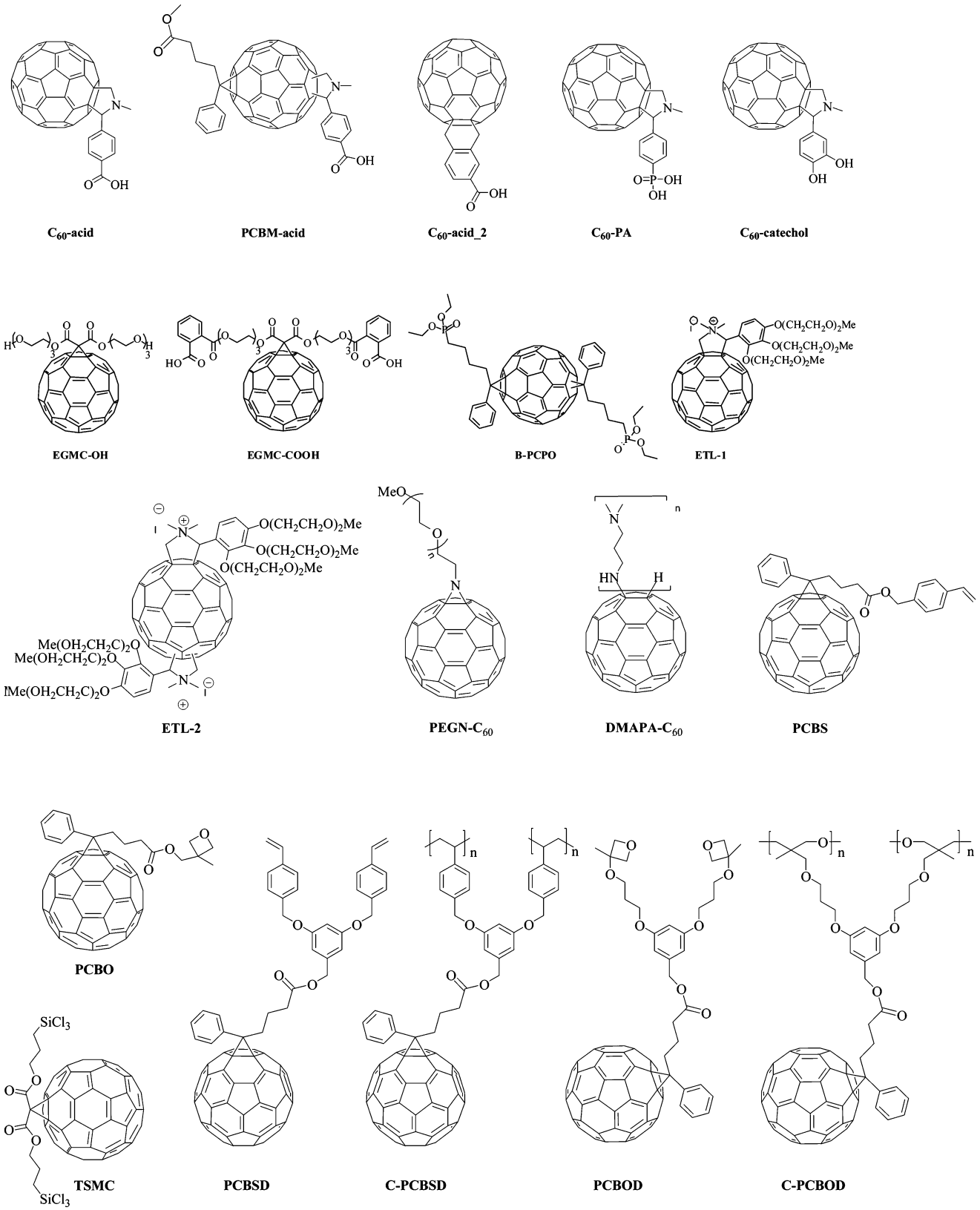

Scheme 2 (*Continued*)

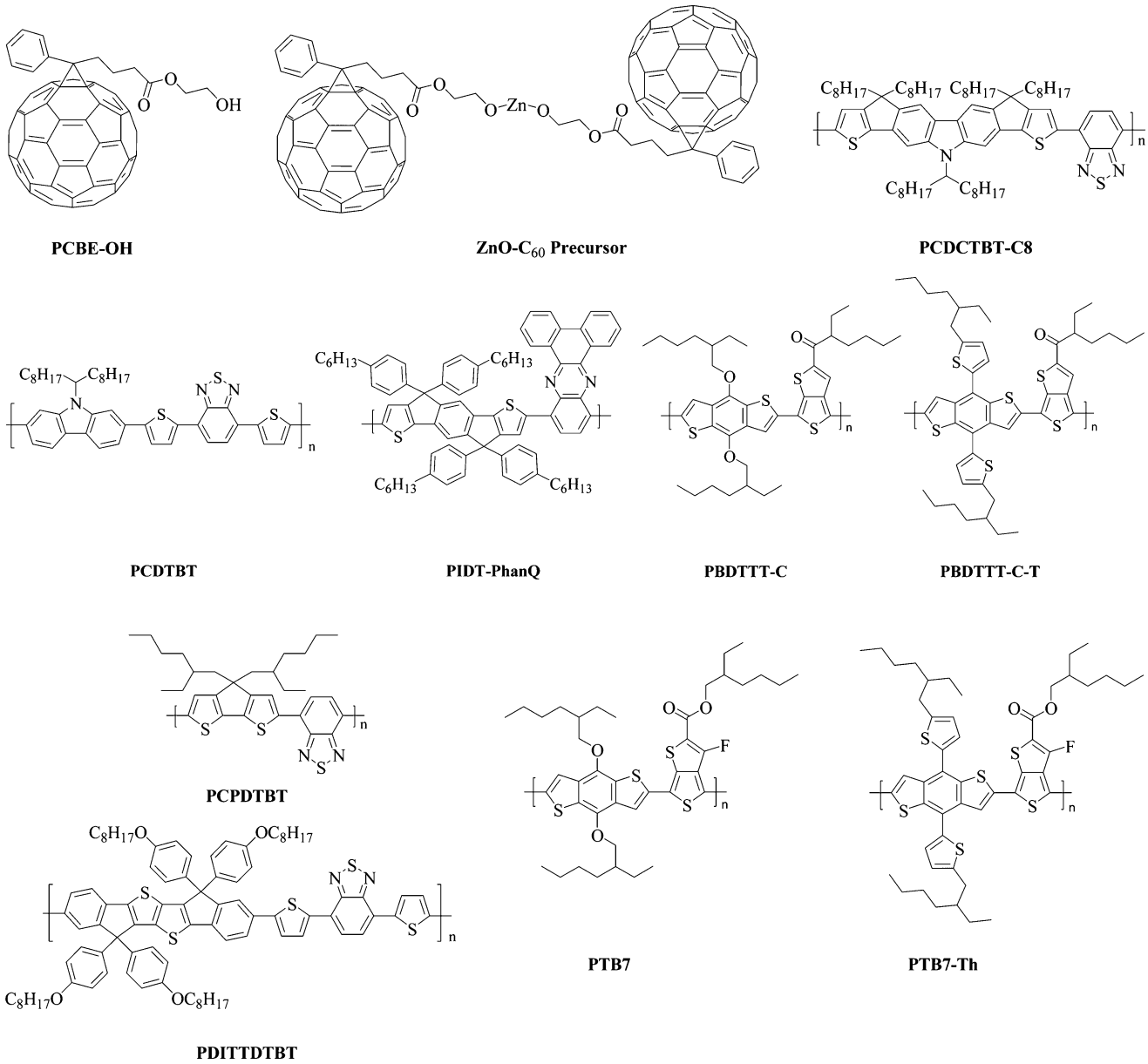

Scheme 2 Structures of fullerene derivatives – C_{60}-acid, PCBM-acid, C_{60}-acid_2, C_{60}-PA, C_{60}-catechol, EGMC–OH, EGMC–COOH, B-PCPO, ETL-1, ETL-2, PEGN-C_{60}, DMAPA-C_{60}, PCBS, PCBO, TSMC, PCBSD, C-PCBSD, PCBOD, C-PCBOD, PCBE-OH, and ZnO–C_{60} precursor and low band-gap polymers – PCDCTBT-C8, PCDTBT, PIDT-PhanQ, PBDTTT-C, PBDTTT-C-T, PCPDTBT, PDITTDTBT, PTB7, and PTB7-Th.

ITO/PEDOT:PSS/active layer/interlayer/Al device configuration, where the active layers are P3HT:$PC_{61}BM$, PBDTTT-C[82] (Scheme 2):$PC_{71}BM$, and PBDTTT-C-T[83] (Scheme 2):$PC_{71}BM$ and the interlayer is either Ca or PEGN-C_{60}. As listed in Table 2 (Entry 15–20), the PEGN-C_{60} based devices all demonstrated comparable device efficiencies to the Ca-based devices. Hence, PEGN-C_{60} can be considered a promising alternative to Ca in conventional PSCs.

3.4 Amine groups

Subsequent to the success of PEGN-C_{60}, an amine-functionalized C_{60} (DMAPA-C_{60}, Scheme 2) was employed as well in regular PSCs to substitute for Ca.[84] The tested active-layer materials are P3HT:$PC_{61}BM$, PBDTTT-C:$PC_{71}BM$, and PBDTTT-C-T:$PC_{71}BM$ and the corresponding devices using DMAPA-C_{60} as the interlayer gave comparable PCE values to those fabricated by use of Ca on the basis of ITO/PEDOT:PSS/active layer/interlayer/Al device structure.[84] (Entry 21–23, Table 2) Moreover, the combination of DMAPA-C_{60} with high work-function metal cathodes, such as Ag, also yielded decent device efficiency (Entry 24, Table 2), offering more flexibility for cathode selection in device fabrication.

3.5 Styrene groups

To realize a multilayer inverted device by cost-effective solution processing, the deposited fullerene derivative interlayer must possess sufficient resistance against the organic solvent used in processing the sequential active layer to prevent interfacial erosion.[85,86] Development of a fullerene material that can be solution-deposited on a substrate and readily undergo chemical

Table 2 Device characteristics of the polymer-based solar cells with interlayer modification

Entry	Active layer	Interlayer	Weight ratio (in wt%)	V_{oc} (V)	J_{sc} (mA cm^{-2})	FF (%)	PCE (%)
1	P3HT/$PC_{61}BM$[a,68]	None	1 : 0.7	0.60	10.07	57.7	3.47
2		C_{60}-acid	1 : 0.7	0.62	11.17	64.1	4.40
3		C_{60}-catehol[b]	1 : 0.7	0.61	11.21	61.0	4.19
4	P3HT/$PC_{61}BM$[c,69]	None	1 : 1	0.60	9.02	67.0	3.61
5		EGMC-OH	1 : 1	0.60	9.43	66.0	3.71
6		EGMC-COOH	1 : 1	0.60	9.61	66.0	3.80
7		EGMC-COOH doped with 40% Li_2CO_3	1 : 1	0.60	10.90	66.0	4.29
8	PCDCTBT-C8:$PC_{71}BM$[c,69]	None	1 : 3	0.72	8.72	57.0	3.63
9		EGMC-COOH doped with 40% Li_2CO_3	1 : 3	0.72	11.10	56.0	4.51
10	PCDTBT:$PC_{71}BM$[d,70]	None	1 : 4	0.71	10.2	56.1	4.83
11		B-PCPO	1 : 4	0.89	9.50	61.7	6.20
12	PIDT-PhanQ:$PC_{71}BM$[e,78]	None	1 : 3	0.74	10.92	57.0	4.61
13		ETL-1	1 : 3	0.87	11.28	64.0	6.28
14		ETL-2	1 : 3	0.88	11.41	66.0	6.63
15	P3HT:$PC_{61}BM$[f,81]	Ca	N/A[g]	0.63	9.01	67.5	3.80
16		PEGN-C_{60}	N/A	0.63	9.21	66.6	3.84
17	PBDTTT-C:$PC_{71}BM$[f,81]	Ca	N/A	0.73	13.80	60.6	6.13
18		PEGN-C_{60}	N/A	0.74	13.99	60.5	6.22
19	PBDTTT-C-T:$PC_{71}BM$[f,81]	Ca	N/A	0.79	14.83	62.4	7.28
20		PEGN-C_{60}	N/A	0.79	14.79	63.4	7.45
21	P3HT:$PC_{61}BM$[f,84]	DMAPA-C_{60}	1 : 0.8	0.63	9.14	67.8	3.88
22	PBDTTT-C:$PC_{71}BM$[f,84]	DMAPA-C_{60}	N/A	0.72	14.08	61.8	6.29
23	PBDTTT-C-T:$PC_{71}BM$[f,84]	DMAPA-C_{60}	1 : 1.5	0.79	14.89	62.9	7.42
24	PBDTTT-C:$PC_{71}BM$[e,84]	DMAPA-C_{60}	N/A	0.73	14.26	59.5	6.20
25	P3HT:$PC_{61}BM$[a,72]	None	1 : 1	0.58	11.60	52.0	3.50
26		C-PCBSD	1 : 1	0.60	12.80	58.0	4.40
27	PCPDTBT:$PC_{71}BM$[a,72]	None	1 : 2	0.48	12.10	32.0	1.90
28		C-PCBSD	1 : 2	0.66	14.50	35.0	3.40
29	P3HT:ICBA[a,50]	None	1 : 1	0.82	10.60	55.0	4.80
30		C-PCBSD	1 : 1	0.84	12.40	60.0	6.22
31	P3HT:ICBA[a,105]	C-PCBSD nanorods	1 : 1	0.84	12.07	72.3	7.30
32		Planar C-PCBSD	1 : 1	0.84	11.17	66.0	6.20
33	P3HT:$PC_{61}BM$[h,113]	None	1 : 1	0.58	10.65	57.76	3.60
34		SA-PCBO	1 : 1	0.60	11.14	60.73	4.10
35		C-PCBOD	1 : 1	0.61	12.25	61.26	4.50
36	P3HT:$PC_{61}BM$[i,122]	None	1 : 1	0.58	9.87	55.00	3.20
37		SA-C-TSMC	1 : 1	0.60	10.42	61.70	3.90
38	PDITTDTBT:$PC_{71}BM$[h,122]	None	1 : 4	0.87	9.94	50.27	4.30
39		SA-C-TSMC	1 : 4	0.91	11.54	55.02	5.80
40	PTB7:$PC_{71}BM$[j,124]	ZnO	1 : 1.5	0.70	13.75	69.00	6.65
41		ZnO-C_{60}	1 : 1.5	0.73	15.41	73.00	8.21
42	PTB7-Th:$PC_{71}BM$[j,124]	ZnO	1 : 1.5	0.79	14.02	69.10	7.64
43		ZnO-C_{60}	1 : 1.5	0.80	15.73	74.30	9.35

[a] ITO/ZnO/interlayer/active layer/PEDOT:PSS/Ag. [b] The C_{60}-SAM was prepared by solution immersion.[68] [c] ITO/PEDOT:PSS/active layer/Ca/Al. [d] ITO/interlayer/active layer/MoO_3/Al. [e] ITO/PEDOT:PSS/active layer/interlayer/Ag. [f] ITO/PEDOT:PSS(40 mm)/active layer/interlayer/Al. [g] Not available. [h] ITO/TiO_x/interlayer/active layer/MoO_3/Ag. [i] ITO/TiO_x/interlayer/active layer/PEDOT:PSS/Ag. [j] ITO/interlayer/active layer/MoO_3/Ag.

cross-linking to form a robust and immobilized layer could be a straightforward and ideal strategy. Styrene is known to be a superb thermally curable group because it can undergo rapid polymerization in the solid state to form polystyrene without the use of any initiators.[87–89] To this end, a fullerene derivative, [6,6]-phenyl-C_{61}-butyric styryl dendron ester, PCBSD (Scheme 2), that contains a small dendron functionalized with two thermally cross-linkable styryl groups was synthesized by our group and the corresponding cross-linked PCBSD (C-PCBSD, Scheme 2) was then integrated into inverted solar devices.[72] A solution of PCBSD was spin-coated on top of the ZnO surface, followed by thermal curing at 160 °C for 30 min. This cross-linked network produced a robust and adhesive thin film with sufficient solvent resistance. A multilayer inverted solar cell based on the ITO/ZnO/C-PCBSD/P3HT:$PC_{61}BM$ (1 : 1, w/w)/PEDOT:PSS/Ag configuration was fabricated and gave a PCE of 4.4% (Entry 26, Table 2). A reference device without the C-PCBSD interlayer gave a PCE of 3.5% (Entry 25, Table 2). With the additional interlayer of C-PCBSD, the PCE was substantially improved by 26%, which results from the simultaneously enhanced V_{oc}, J_{sc}, and FF relative to the device without interlayer. The use of the C-PCBSD interlayer provides an extra P3HT/C-PCBSD interface area for ultrafast exciton dissociation, which is more efficient than the P3HT/ZnO interface.[90,91] Moreover, the

LUMO energy level of C-PCBSD (3.8 eV) is located between the LUMO of P3HT (3.3 eV) and the conduction band of ZnO (4.4 eV). Therefore, the C-PCBSD can function as an energy gradient intermediate, so that electrons can be efficiently transported to the ZnO through an energetically downhill cascade pathway.[92]

The device stability was also examined.[72] The PCEs of the unencapsulated inverted solar cell devices were periodically measured for 35 days to monitor their long-term stability. With the presence of the C-PCBSD interlayer, the device lifetime was enhanced by 1.5 time. Device degradation is known to be related to leakage current caused by the formation of hot spots in bulk or at the interface.[93] The coverage of a three-dimensional C-PCBSD network on ZnO might passivate the hot spots generated in the ZnO to suppress the leakage current, thus improving the operational lifetime. Additionally, without this interlayer as a dense and robust spacer, gradual mutual penetration between the ZnO and the active layer may alter their chemical or physical properties as the operational time increases.

This strategy was also applied to other blending systems. A inverted device based on ITO/ZnO/C-PCBSD/PCPDTBT[94,95] (Scheme 2):$PC_{71}BM$ (1 : 2, w/w)/PEDOT:PSS/Ag was fabricated and exhibited a V_{oc} of 0.66 V, a J_{sc} of 14.50 mA cm^{-2}, and an FF of 35%, leading to a PCE of 3.4% (Entry 28, Table 2), which has a considerable improvement of 78% compared to the reference device without the C-PCBSD interlayer (Entry 27, Table 2). Moreover, the utilization of n-type bis-adduct fullerenes in an inverted device with the C-PCBSD interlayer modification was also carried out.[50] ICBA was selected as the n-type materials on account of its high-lying LUMO level that has been demonstrated to be beneficial for the enhancement of V_{oc}.[49] A device on the basis of ITO/ZnO/C-PCBSD/P3HT:ICBA (1 : 1, w/w)/PEDOT:PSS/Ag configuration exhibited a V_{oc} of 0.84 V, J_{sc} of 12.4 mA cm^{-2}, and FF of 60%, achieving a high PCE of 6.22% (Entry 30, Table 2), which is a 29% increase over the reference device without the C-PCBSD interlayer (Entry 29, Table 2).

To provide a direct path for charge transport while maintaining a large interfacial area in BHJ solar cells, the ideal architecture of the donor and acceptor is the periodic, vertically aligned, and interpenetrating ordered bulk heterojunction (OBHJ).[1,96–101] C-PCBSD combined with the anodic aluminum oxide (AAO) template-assisted approach[102–104] was employed to construct a well-organized nanostructured interface. A device on the basis of ITO/ZnO/C-PCBSD nanorods/P3HT:ICBA/PEDOT:PSS/Ag configuration was completed (Fig. 2).[105] Under otherwise identical conditions, a control device, by using the ITO/ZnO/planar C-PCBSD/P3HT:ICBA/PEDOT:PSS/Ag configuration (without the C-PCBSD nanostructure), was fabricated for comparison. The device with the C-PCBSD nanorods exhibited an exceptional PCE of 7.3%, with V_{oc} = 0.84 V, J_{sc} = 12.07 mA cm^{-2}, and FF = 72.3% (Entry 31, Table 2). The control device without the C-PCBSD nanostructure exhibited an inferior PCE of 6.2%, with a V_{oc} of 0.84 V, a J_{sc} of 11.17 mA cm^{-2}, and an FF of 66% (Entry 32, Table 2). The efficiency enhancement could be ascribed to the fact that the array of C-PCBSD nanorods penetrating into the BHJ layer offers substantial P3HT/C-PCBSD interfacial area for extra exciton dissociation, thereby generating a higher photocurrent, which was supported by steady-state photoluminescence (PL) measurements.[105] Furthermore, the introduction of C-PCBSD nanorods enhanced the electron mobility from 9.4×10^{-4} to 2.6×10^{-3} cm^2 V^{-1} s^{-1} while maintaining the hole mobility value of approximately 3×10^{-3} cm^2 V^{-1} s^{-1}, thus leading to more balanced charge transport. Such an enhancement in electron mobility has also been demonstrated in previous studies, showing that nanostructured organic semiconductors can possess superior charge-transport properties than their planar counterparts.[99,100,107,108]

The stability of the devices without encapsulation was also evaluated. The device stability was enhanced significantly with the help of the C-PCBSD nanorods. As suggested by optical microscopy, the macrographic alteration of the active-layer morphology is the primary reason causing the reduction of efficiency of the devices. Considering that a part of the P3HT:ICBA BHJ infiltrated into the C-PCBSD nanorods and is thus surrounded and confined between the rods, nanostructure-assisted morphological stability could be rationalized by the spatial confinement effect, which might suppress the thermal-driven crystallization of ICBA and P3HT upon thermal annealing.

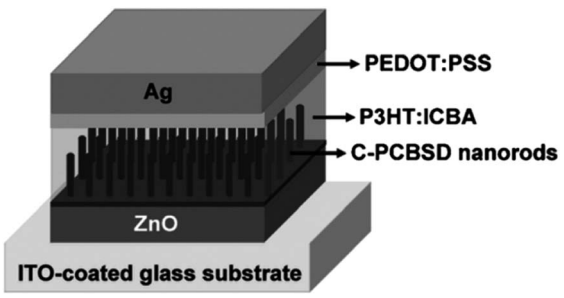

Fig. 2 Schematic representation of the nano-structured device architecture. Reprinted with permission from ref. 105. Copyright 2011, Wiley-VCH Verlag GmbH & Co. KGaA.

3.6 Oxetane groups

Oxetane functional group has been extensively utilized as an efficient cross-linker for the applications of organic electronics.[88,106–111] In comparison to the radical polymerization of styrene, cationic polymerization of oxetane is less sensitive to air. Moreover, it is reasonable to postulate that hydroxyl groups on metal oxide can also serve as nucleophiles to open the ring of protonated oxetane, thereby forming a monolayer modifier by covalent bonding.[112]

We developed a $PC_{61}BM$-based n-type material, [6,6]-phenyl-C_{61}-butyric oxetane dendron ester (PCBOD) (Scheme 2), functionalized with a small dendron containing two oxetane groups as the cross linkers.[113] To induce cationic oxetane ring-opening polymerization, a catalytic amount of photoacid generator (PAG) is required to generate acidic protons upon UV irradiation. Infrared spectroscopy suggested that when the polymerization temperature is above the glass transition temperature (T_g) of PCBOD, the two arms of the dendron can provide adequate flexibility for the oxetane groups to react in the solid state to furnish cross-linked PCBOD (C-PCBOD) (Scheme 2). A plausible mechanism was proposed to account for the self-

assembled monolayer and cross-linking of PCBOD on the TiO_x surface (Fig. 3).[113,114] The anchoring of oxetane groups may take place by nucleophilic attack of the hydroxyl groups on the TiO_x surface to open the protonated oxetane rings. Further bidentate anchoring is possible through the etherification condensation. Once the self-assembled monolayer is formed, the intermolecular cross-linking can efficiently occur through ring-opening polymerization between the oxetane groups to vertically grow a multi-molecular interlayer.

Subsequently, inverted solar cell devices based on the configuration of ITO/TiO_x/interlayer/P3HT:$PC_{61}BM$ (1 : 1, w/w)/MoO_3/Ag was fabricated.[113] The device with the C-PCBOD interlayer exhibited a V_{oc} of 0.61 V, a J_{sc} of 12.25 mA cm^{-2}, and an FF of 61.26%, achieving a PCE of 4.5% (Entry 35, Table 2). The device without the C-PCBOD layer delivered an inferior PCE of 3.6% (Entry 33, Table 2). Noticeably, when PCBOD was replaced with PCBO (Scheme 2) to form a self-assembly PCBO monolayer (SA-PCBO), the corresponding device gave a PCE of 4.10% (Entry 34, Table 2), which drops by 10% compared to the C-PCBOD-based device. This result suggests that a dense, robust, and pinhole-free multimolecular interlayer is capable of further strengthening the interface characteristics.

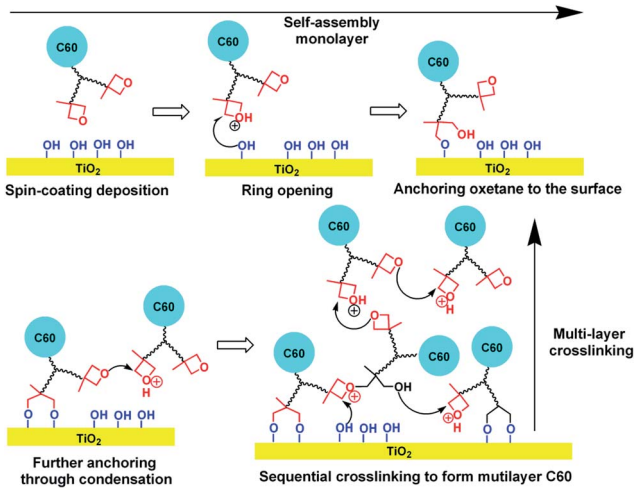

Fig. 3 Proposed mechanism for self-assembly and multi-molecular cross-linking of PCBOD on the TiO_x surface. Reprinted with permission from ref. 114. Copyright 2011, American Chemical Society.

3.7 Trichlorosilane

Trichlorosilane moieties are known to readily undergo facile hydrolysis to produce polysiloxane in ambient air. Because of its high reactivity and wide availability, it is frequently used to implement self-assembly and/or cross-linking for the purpose of surface modification.[115–121] We recently have incorporated trichlorosilane functionalities into fullerene derivatives for PSC applications. Bis(2-(trichlorosilyl)propyl)-malonate C_{60} (TSMC, Scheme 2) containing two trichlorosilane groups was synthesized and spin-cast on top of the ITO/TiO_x surface to form a self-assembled/cross-linked network of TSMC (SA-C-TSMC).[122] Atomic force microscopy (AFM) was employed to investigate the surface morphology. In AFM images, pronounced nanostructures were found on the surface of the SA-C-TSMC layer with a RMS roughness of 5.26 nm.[122] These vertically grown semispherical nanoaggregates comprising the cross-linked TSMC aggregates are *ca.* 10–30 nm in height and *ca.* 20–60 nm in diameter. In contrast, the surface of the pristine TiO_x exhibited much smooth morphology with a RMS roughness *ca.* 3.49 nm. A plausible mechanism accounting for the formation of SA-C-TSMC layer on the top of TiO_x surface is proposed in Fig. 4. Upon spin-coating, the nucleophilic hydroxyl groups on

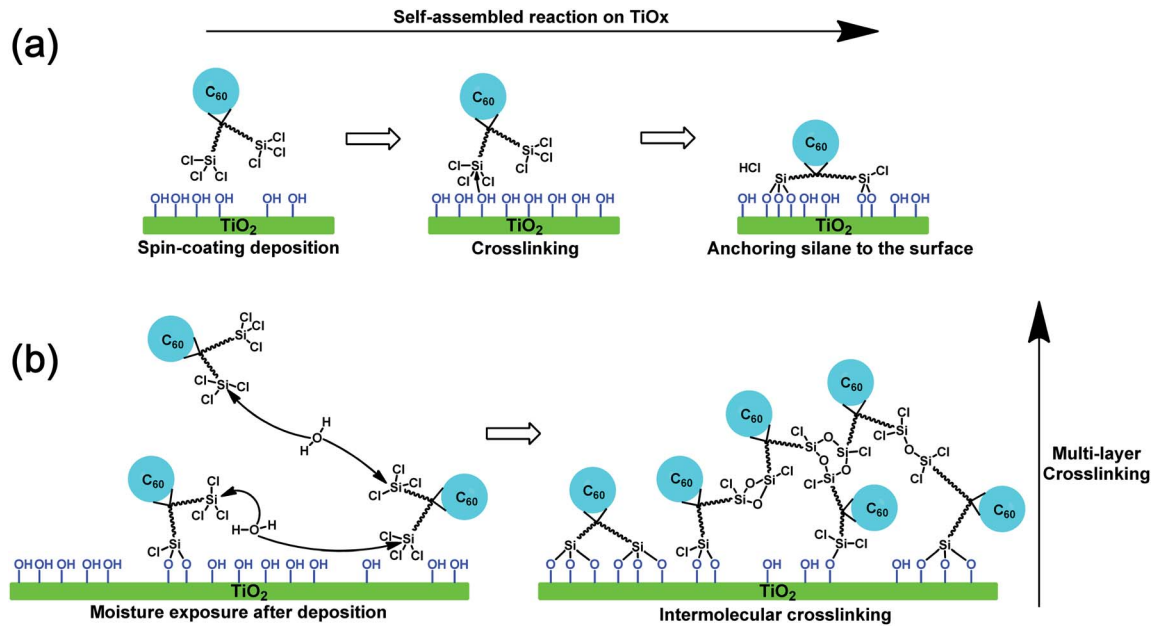

Fig. 4 Hydrolysis of the trichlorosilane groups of TSMC: (a) self-assembled reaction on TiO_x, (b) intermolecular cross-linking to form multilayer network. Reprinted with permission from ref. 123. Copyright 2013, American Chemical Society.

the surface can attack the electrophilic silicon atoms of trichlorosilanes to spontaneously form a self-assembled monolayer *via* the Ti–O–Si linkages (Fig. 4a). In the mean time, intermolecular cross-linking between the TSMC molecules to form a multilayer network through the siloxane Si–O–Si linkages also proceeds efficiently (Fig. 4b). Considering that hydrolysis of trichlorosilane groups with moisture is a fast and energetically favorable process, it is reasonable to expect that some of the TSMC molecules have started cross-linking and aggregating into nanoparticles suspended in the solution before spin-casting. The precross-linked nanoparticles deposited on the surface were integrated into the SA-C-TSMC layer, thereby forming the vertically aligned nanostructures on the surface. The nanoaggregates on the SA-C-TSMC layer can provide extra charge-generating interfacial area and straight electron transport pathways.

A multilayer inverted device with the configuration of ITO/TiO_x/SA-C-TSMC/P3HT:$PC_{61}BM$ (1 : 1, w/w)/PEDOT:PSS/Ag was fabricated. It exhibited a V_{oc} of 0.60 V, a J_{sc} of 10.42 mA cm^{-2}, an FF of 61.70%, and a PCE of 3.9% (Entry 37, Table 2), which represents a 22% improvement over the device without the SA-C-TSMC layer (PCE = 3.2%, Entry 36, Table 2). This strategy was further applied to the devices incorporating various photoactive materials. A p-type copolymer PDITTDTBT[123] (Scheme 2) was chosen to test the general applicability of SA-C-TSMC. The device with the SA-C-TSMC interlayer (ITO/TiO_x/SA-C-TSMC/PDITTDTBT:$PC_{71}BM$ (1 : 4, w/w)/MoO_x/Ag) and its corresponding control device in the absence of the interlayer were thus fabricated. Compared to the device without SA-C-TSMC (Entry 38, Table 2), the device with SA-C-TSMC exhibited V_{oc} = 0.91 V, J_{sc} = 11.54 mA cm^{-2}, FF = 55.02% and PCE = 5.8% (Entry 39, Table 2), which is a considerable enhancement of 35% in efficiency. Furthermore, this experiment also demonstrates that the TSMC interlayer is effective not only for the $PC_{61}BM$-based system but also for the $PC_{71}BM$-based system.

3.8 ZnO doped with fullerene materials

The combination of fullerenes and metal oxides in PSCs is an intriguing idea. Lately it has been realized by employing ZnO doped with PCBE-OH (Scheme 2) as the cathode in inverted PSCs.[124] This fullerene-doped ZnO film (abbreviated as ZnO-C_{60}) was prepared by spin coating a mixture of PCBE-OH (0.5 wt%) and $Zn(OAc)_2$ (99.5 wt%) in 2-methoxyethanol and ethanolamine on ITO, followed by sintering at 180 °C under ambient conditions. It is believed that a condensation reaction would first occur between $Zn(OAc)_2$ and PCBE-OH to form a Zn-C_{60} precursor (Scheme 2). Contact angle and XPS measurements suggest that the formed ZnO-C_{60} film is fullerene-rich on its surface, indicating that the fullerene molecules are mainly situated at the uppermost part of the ZnO-C_{60} film. The HOMO and LUMO energy levels of the ZnO-C_{60} film were determined to be −7.01 and −4.53 eV by UV-Vis spectroscopy. For the pristine ZnO film, the HOMO and LUMO energy levels are −7.24 and −4.14 eV, respectively. It is evident that the doping of PCBE-OH to ZnO results in smaller energy band gap, accompanied by the upshift of the HOMO energy and the downshift of the LUMO energy. The observed energy variation also reflects with the fact that the fullerenes are located on the surface of the ZnO-C_{60} film, thus leading to the change of the frontier-orbital energies. Furthermore, the electron mobility and surface conductivity of the ZnO-C_{60} film were evaluated as well and found to be appreciably higher than those of the pristine ZnO film.

Subsequently, the ITO/interlayer/active layer/MoO_3/Ag device configuration was employed to examine the effect brought by the ZnO-C_{60} film, where the cathodic interlayer is either pristine ZnO or ZnO-C_{60} film and the active layer is PTB7[125] (Scheme 2):$PC_{71}BM$ or PTB7-Th[124] (Scheme 2):$PC_{71}BM$. The device characteristics are listed in Table 2. Evidently, the device efficiencies increased significantly when the cathodic interlayer varied from pristine ZnO to ZnO-C_{60}. The best PCE of 9.35% was achieved by use of the ITO/ZnO-C_{60}/PTB7-Th:$PC_{71}BM$/MoO_3/Ag device structure. As concluded from the attained experimental data, the success of this fullerene-dopant strategy mainly lies in the enhancement of electron collection of the cathode and the diminution of the interfacial series resistance between the cathode and the active layer.

4. Morphological stabilization

Morphological instability of PSCs is considered to be one of the major obstacles hindering their path toward commercialization. However, the development of practicable strategies to preserve optimal morphology is rather challenging. Fréchet and co-workers found that a slight decrease of the regioregularity of P3HT to weaken the crystallization-driven phase separation not only retains the device efficiency but also enhances the thermal stability of morphology in the solar cells.[43] Moreover, Fréchet *et al.* used a diblock copolymer containing fullerene and oligothiophene pendant groups to serve as a compatibilizer to improve adhesion between the P3HT and $PC_{61}BM$ boundaries.[126] Wudl and co-workers also used similar strategy to adjust the interfacial morphology between P3HT and $PC_{61}BM$ and found a substantial improvement in device performance.[127] Lately, several elegant approaches, including *in situ* polymerization,[63] polyethylene glycol (PEG) end-capped fullerene,[128] supramolecular pentafluorophenyl-fullerene interactions,[129] and light-induced oligomerization of fullerenes[130] have been utilized in stabilizing the active-layer morphology and simultaneously retaining the device efficiency, providing insight into the general applicability of morphological stabilization.

4.1 *In situ* polymerization

One of the most straightforward methods for stabilization of the active-layer morphology is to lock it by covalent bonding.[131–135] *In situ* chemical cross-linking in BHJ films right after the formation of the optimal morphology is an ideal strategy to achieve this goal.[131–135] Crosslinkable PCBSD (Scheme 2) with two styryl groups can not only be used in interfacial modification,[72] but also be utilized in active layers for morphological stabilization.[63] Conventional devices on the basis of ITO/PEDOT:PSS/active layer/Ca/Al configuration were manufactured. Various amounts of PCBSD were doped into the

P3HT:$PC_{61}BM$ blend. The blending weight ratio of P3HT to the total n-type materials (*i.e.*, $PC_{61}BM$ plus PCBSD) was fixed at 1 : 1 and the relative proportion between the $PC_{61}BM$ and PCBSD was adjusted. Two-stage thermal annealing as the standard procedure for all blending systems was implemented.[63] The spin-coated active-layer blend was initially thermally annealed at 110 °C for 10 min to develop suitable morphology, followed by thermal annealing at 150 °C for another 10 min to trigger *in situ* polymerization. It was found that by doping small amounts of PCBSD into the P3HT:$PC_{61}BM$ blend (P3HT:$PC_{61}BM$:PCBSD = 6 : 5 : 1 in weight), the initial morphology of the blend can be fixed and preserved effectively after polymerization. The device based on this blend showed highly stable device characteristics, delivering a PCE of 3.70% during 25 h isothermal heating at 150 °C (Entry 4, Table 3). In sharp contrast, under otherwise identical conditions, the P3HT:$PC_{61}BM$ blend underwent severe phase separation due to the crystallization of P3HT and the aggregation of $PC_{61}BM$. The PCE of the P3HT:$PC_{61}BM$-based device dropped dramatically from 4.08% to 0.69% (Entry 1 and 2, Table 3). PCBS (Scheme 2) with only one styryl moiety, was also used as a dopant in the active layer. At a low doping concentration of PCBS in the blend (P3HT:$PC_{61}BM$:PCBS = 6 : 5 : 1 in weight), linearly polymerized PCBS can also stabilize the morphology against heating. This device exhibited a PCE of 3.61% during 25 h heating at 150 °C (Entry 6, Table 3).[63]

4.2 Polyethylene glycol (PEG) end-capped fullerene

Fullerenes are usually insoluble in polar solvent, such as water.[136,137] However, when they are functionalized with hydrophilic PEG groups, the resultant fullerene derivatives often have high solubility in polar solvents.[128] A PEG-end capped $PC_{61}BM$ derivative, PCBPEG (Scheme 3), was developed and used as a dopant to stabilize the morphology of the P3HT:$PC_{61}BM$ blend. By employing the ITO/PEDOT:PSS/active layer/Al configuration, when the P3HT/$PC_{61}BM$ active-layer blend was doped with 5 wt % of PCBPEG, the corresponding device gave a V_{oc} of 0.60 V, a J_{sc} of 11.44 mA cm^{-2}, an FF of 60.0%, and a PCE of 4.15%. After being heated at 60 °C for 300 h, the device can still maintain 50% of the original PCE value. For comparison, the device without doping of PCBPEG lost more than 85% of its original PCE value after 300 h heating at 60 °C. Transmission electron microscopy reveals that PCBPEG is able to suppress the formation of large-scale $PC_{61}BM$ aggregation at elevated temperatures, thus restraining the P3HT/$PC_{61}BM$ from severe phase separation at elevated temperatures.

4.3 Supramolecular pentafluorophenyl-fullerene interactions

It has been reported by Nakamura and co-workers that through the pentafluorophenyl (C_6F_5)-fullerene interaction, 1,4-bis-(pentafluorobenzenyl) fullerene assembles into an interlocked one-dimensional zigzag array in the solid state.[138] It is intriguing to further utilize this C_6F_5–C_{60} interaction in stabilizing the active-layer morphology in PSCs. To this end, we developed a new $PC_{61}BM$-based fullerene, [6,6]-phenyl-C_{61} butyric acid pentafluorophenyl ester ($PC_{61}BP^F$, Scheme 3) and tested it in conventional solar devices (ITO/PEDOT:PSS/active layer/Ca/Al).[129] A series of active-layer blends with different doping ratio of $PC_{61}BP^F$ were initially thermally annealed at 140 °C for 15 min, and then subjected to isothermal heating at 150 °C for the longest 25 hours prior to the deposition of top electrodes. It was found that by doping small amounts of $PC_{61}BP^F$ into the P3HT:$PC_{61}BM$ blend (P3HT:$PC_{61}BM$:$PC_{61}BP^F$ = 6 : 5 : 1

Table 3 Photovoltaic parameters of PSCs based on various blends isothermally heated at 150 °C for different time

Entry	Blend	Weight ratio (in wt%)	Time (h)	V_{oc} (V)	J_{sc} (mA cm^{-2})	FF (%)	PCE (%)
1	P3HT/$PC_{61}BM$	1 : 1	—	0.60	10.26	66	4.08
2			25	0.62	2.27	49	0.69
3	P3HT/$PC_{61}BM$/PCBSD	6 : 5 : 1	—	0.60	8.44	66	3.32
4			25	0.60	9.35	66	3.70
5	P3HT/$PC_{61}BM$/PCBS	6 : 5 : 1	—	0.60	9.82	65	3.84
6			25	0.58	9.49	66	3.61

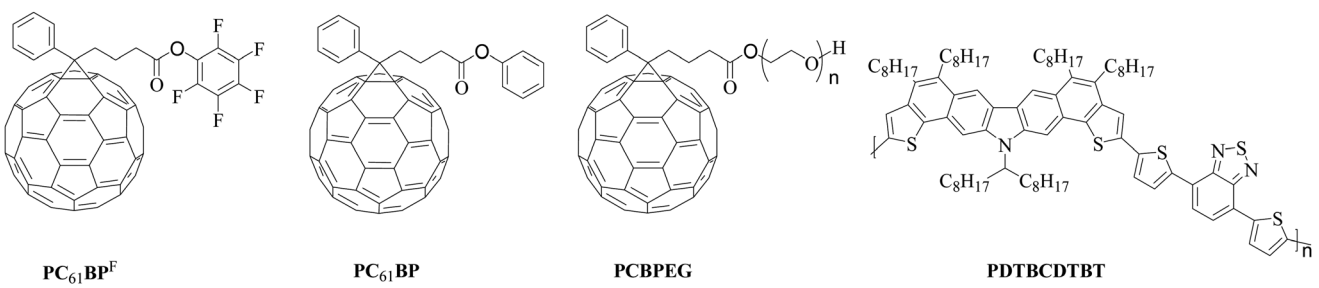

Scheme 3 Chemical structures of $PC_{61}BP^F$, $PC_{61}BP$, PCBPEG, and PDTBCDTBT.

Table 4 Photovoltaic parameters of PSCs (ITO/PEDOT:PSS/active layer/Ca/Al) before and after isothermal heating at 150 °C for 25 h

Entry	Blend	Weight ratio (in wt%)	Time (h)	V_{oc} (V)	J_{sc} (mA cm^{-2})	FF (%)	PCE (%)
1	P3HT:$PC_{61}BM$	1 : 1	0	0.60	−10.26	66.00	4.08
2			25	0.62	−2.27	49.00	0.69
3	P3HT:$PC_{61}BM$:$PC_{61}BP^F$	6 : 5 : 1	0	0.60	−9.87	65.60	3.88
4			25	0.62	−9.06	65.47	3.68
5	P3HT:$PC_{61}BM$:$PC_{61}BP$	6 : 5 : 1	0	0.60	−8.92	64.40	3.45
6			25	0.62	−1.78	41.48	0.44

in weight), the device performance showed highly stable device characteristics, delivering a PCE of 3.68% (Entry 4, Table 4) after 25 h isothermal heating at 150 °C. In sharp contrast, the PCE of the P3HT:$PC_{61}BM$ blend dropped dramatically from 4.08% (Entry 1, Table 4) to 0.69% (Entry 2, Table 4) after 25 h isothermal heating. The decreased efficiency is mainly a result of the decrease of J_{sc} value. In comparison to $PC_{61}BP^F$, $PC_{61}BP$ (Scheme 3) with non-fluorinated phenyl group was synthesized and also used as the doping component in the P3HT:$PC_{61}BM$ blend. By using the same doping ratio (P3HT:$PC_{61}BM$:$PC_{61}BP$ = 6 : 5 : 1 in weight), the device yielded a PCE of 3.45% initially (Entry 5, Table 4). Subsequent to 25 h thermal heating at 150 °C, it degraded significantly to 0.44% (Entry 6, Table 4). These results clearly demonstrate that the presence of pentafluorophenyl group in $PC_{61}BP^F$ to exert C_6F_5–C_{60} interactions plays a decisive role in controlling and stabilizing the morphology against thermal heating.

A rational mechanism for the morphological stabilization of the P3HT:$PC_{61}BM$:$PC_{61}BP^F$ blends is proposed and illustrated in Fig. 5. For the as-cast thin films with dopant of $PC_{61}BP^F$, diffusion of the fullerene molecules dispersed in the mixed regions is partially restricted by the intermolecular C_6F_5–C_{60} interactions, reducing their tendency toward thermal-induced fullerene aggregation (Fig. 5a). Pre-annealing at 140 °C for 15 min may not be sufficient to achieve optimized morphology, which depends on the loading amount of $PC_{61}BP^F$ (Fig. 5b). By further heating at 150 °C during 25 h, the fullerene molecules in the mixed regions might gradually overcome the supramolecular attraction and slowly aggregate into fullerene clusters with concurrent enhancement of P3HT crystallinity (Fig. 5c). DFT calculations at the wB97XD/6-311G(d,P) level of theory was employed to investigate the stabilization brought by the pentafluorophenyl group of $PC_{61}BP^F$.[129] The computational results reveal that the C_{60} core can interact with the pentafluorophenyl group to form a stable adduct and this intermolecular interaction was estimated to be −10.58 kcal mol^{-1}. The presence of C_6F_5–C_{60} interactions is thus supported by DFT calculations.

This strategy was also applied to other blending systems. A device on the basis of the ITO/PEDOT:PSS/PDTBCDTBT[139] (Scheme 3):$PC_{71}BM$ (2 : 3 in wt%)/Ca/Al configuration was fabricated. The active layer, thermally annealed at 100 °C for 10 min, achieved a high efficiency of 5.34%. After isothermal heating of the active layer at 150 °C for 24 h, the efficiency dramatically degraded to an extremely low value of 0.01%. Under otherwise identical conditions, the device by adding 10 wt% $PC_{61}BP^F$ into the active layer delivered an initial efficiency of 5.24%, indicating that the incorporation of $PC_{61}BP^F$ into this system does not alter the device performance. In sharp contrast, after thermal annealing at 150 °C for 25 h, this $PC_{61}BP^F$-incorporated device still achieved a comparable PCE of 4.24%, that is about 81% of its original value.

4.4 Light induced oligomerization of fullerenes

Photoinduced oligomerization of fullerenes *via* [2 + 2] cycloaddition has been demonstrated.[140] Lately, this concept has been incorporated into PSCs with the aim of ensuring thermally stable D–A morphology.[130] The morphological behaviour of PCDTBT (Scheme 2):$PC_{61}BM$ blend was investigated. The as-cast PCDTBT:$PC_{61}BM$ blend film was illuminated under

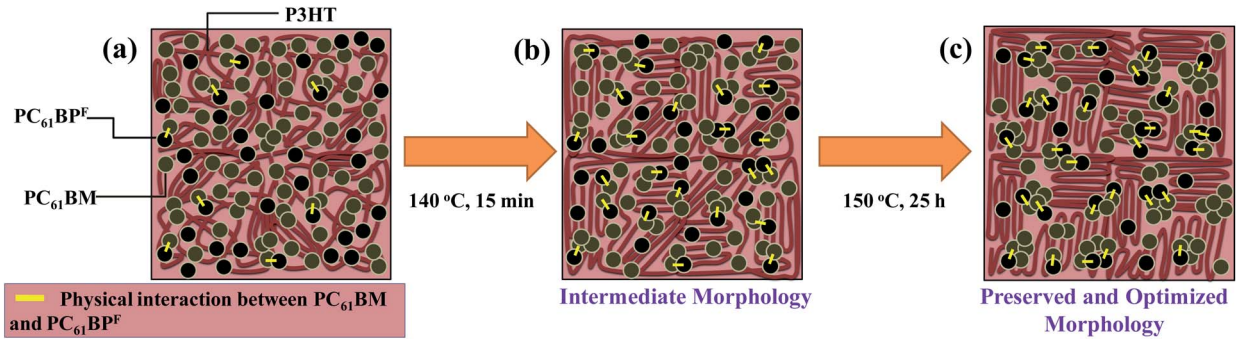

Fig. 5 Morphological stabilization of P3HT:$PC_{61}BM$:$PC_{61}BP^F$ blends. Reprinted with permission from ref. 129. Copyright 2013, Wiley-VCH Verlag GmbH & Co. KGaA.

nitrogen for various time periods by a moderate fluorescent lamp with intensity of 10 mW cm^{-2}. No apparent morphological change subsequent to thermal stress at 140 °C for 1 h was observed for the blend pre-treated by the above-mentioned light exposure. In sharp contrast, the blend without light exposure underwent fast growth of $PC_{61}BM$ crystallites under otherwise identical thermal stress conditions. The enhanced morphological stability is attributed to the formation of small-domain $PC_{61}BM$ oligomers that minimize the diffusion of $PC_{61}BM$ out of polymer matrix. The device stability were then examined on the basis of the ITO/PEDOT:PSS/PCDTBT:$PC_{61}BM$ (1 : 2) (with or without >120 min light exposure)/Ca/Al. The initial efficiencies for the devices with or without illumination are about 6%, suggesting that the illumination step does not have negative effect on the device performance. Overall, the device stability under thermal stress at 80 °C was enhanced nearly 10 fold through the pre-treatment of light exposure. The application of this approach to other blends, such as DPP-TT-T[141]/$PC_{61}BM$, was demonstrated as well, suggesting its general applicability.

5. Conclusions

Research effort devoted to the field of bulk heterojunction (BHJ) polymer solar cells (PSCs) has delivered promising results. Nevertheless, in order to achieve the ultimate goal of commercialization, further optimization is certainly required. Herein we reviewed the research progress on applications of fullerene-based materials in the BHJ PSCs. It was categorized into three areas: bis-adduct fullerenes, fullerene-based interlayer modification, and morphological stabilization. For bis-adduct fullerenes, the second functionalization on the core structure of the mono-substituted C_{60} can reduce the π-conjugation and electron delocalization in the C_{60}, resulting in the formed bis-adduct C_{60} derivatives with larger electrochemical reduction potentials and thus higher-lying LUMO levels. These bis-adduct fullerenes, *i.e.* bisPCBM, ICBA, $IC_{70}BA$, IPCBM, bis-TOQC, and DMPCBA, were used in BHJ PSCs and found to be effective in increasing the V_{oc} of the corresponding devices, in turn enhancing the PCE values. Moreover, the function of bis-adduct fullerenes is not merely limited in the enlargement of V_{oc}. For example, due to the amorphous nature of DMPCBA, the morphology of the P3HT:DMPCBA blend can be preserved after long-term thermal heating.

As for interlayer modification, incorporation of an additional n-type fullerene interlayer between inorganic and organic active layers either in regular or inverted solar cells can help in minimization of charge recombination losses at the interface and improvement of charge transfer from the active layer to the inorganic layer, thus resulting in higher PCEs. To this end, various functional groups, such as acid, alcohol, phosphoric ester, polyethylene glycol, amine, styrene, oxetane, trichlorosilane, and ZnO were employed to modify fullerenes, respectively, and the resultant fullerenes exhibited promising interfacial electronic properties in the improvement of device characteristics. Certain fullerene, such as cross-linked PCBSD (C-PCBSD) can increase the device stability since the hot spots generated in the inorganic layer (ZnO) may be passivated by the cross-linked PCBSD interlayer and the leakage current is therefore suppressed, giving rise to longer device operational lifetime. Noteworthily, the incorporation of the anodic aluminum oxide template with C-PCBSD can not only increase the device efficiency but also the device stability. The efficiency enhancement could be ascribed to the fact that the C-PCBSD nanostructures penetrating into the BHJ layer offer substantial P3HT/C-PCBSD interfacial area for extra exciton dissociation, thereby generating a higher photocurrent and PCE. The morphological stability may result from the spatial confinement effect, which might suppress the thermal-driven crystallization of ICBA and P3HT upon thermal annealing.

Lastly, with regard to morphological stability, *in situ* polymerization was applied to lock the optimal morphology by covalent bonding. Functionalized fullerenes in which the functional groups are polyethylene glycol and perfluorophenyl moieties were utilized to suppress the thermal-induced fullerene aggregation. Light-induced oligomerization of $PC_{61}BM$ was demonstrated to be effective in minimizing the aggregation of $PC_{61}BM$ under thermal stress. These strategies can enhance the device stability significantly since the optimal active-layer morphologies are more robust and therefore less sensitive towards thermal heating.

The research of employing fullerene derivatives in BHJ PSCs has established many valuable landmarks. It is envisioned that further investigation and advancement in this field can increase both the device efficiency and stability and ultimately reach the goal of commercialization.

Acknowledgements

We thank the Ministry of Science and Technology and the Ministry of Education, and Center for Interdiscplinary Science (CIS) of the National Chiao Tung University, Taiwan, for financial support. Y. J. C thanks the support from the Golden-Jade fellowship of the Kenda foundation, Taiwan.

Notes and references

1 K. M. Coakley and M. D. McGehee, *Chem. Mater.*, 2004, **16**, 4533.
2 S. Günes, H. Neugebauer and N. S. Sariciftci, *Chem. Rev.*, 2007, **107**, 1324.
3 J. J. M. Halls, K. Pichler, R. H. Friend, S. C. Moratti and A. B. Holmes, *Appl. Phys. Lett.*, 1996, **68**, 3120.
4 M. Theander, A. Yartsev, D. Zigmantas, V. Sundström, W. Mammo, M. R. Andersson and O. Inganäs, *Phys. Rev. B: Condens. Matter*, 2000, **61**, 12957.
5 A. Haugeneder, M. Neges, C. Kallinger, W. Spirkl, U. Lemmer, J. Feldmann, U. Scherf, E. Harth, A. Gügel and K. Müllen, *Phys. Rev. B: Condens. Matter*, 1999, **59**, 15346.
6 T. Stübinger and W. Brütting, *J. Appl. Phys.*, 2001, **90**, 3632.
7 D. E. Markov, E. Amsterdam, P. W. M. Blom, A. B. Sieval and J. C. Hummelen, *J. Phys. Chem. A*, 2005, **109**, 5266.
8 Y.-J. Cheng, S.-H. Yang and C.-S. Hsu, *Chem. Rev.*, 2009, **109**, 5868.

9 W. Ma, C. Yang, X. Gong, K. Lee and A. J. Heeger, *Adv. Funct. Mater.*, 2005, **15**, 1617.
10 A. C. Mayer, S. R. Scully, B. E. Hardin, M. W. Rowell and M. D. McGehee, *Mater. Today*, 2007, **10**, 28.
11 G. Li, V. Shrotriya, J. Huang, Y. Yao, T. Moriarty, K. Emery and Y. Yang, *Nat. Mater.*, 2005, **4**, 864.
12 M. Reyes-Reyes, K. Kim and D. L. Carroll, *Appl. Phys. Lett.*, 2005, **87**, 083506.
13 C. H. Woo, B. C. Thompson, B. J. Kim, M. F. Toney and J. M. J. Fréchet, *J. Am. Chem. Soc.*, 2008, **130**, 16324.
14 C. J. Brabec, A. Cravino, D. Meissner, N. S. Sariciftci, T. Fromherz, M. T. Rispens, L. Sanchez and J. C. Hummelen, *Adv. Funct. Mater.*, 2001, **11**, 374.
15 M. C. Scharber, D. Mühlbacher, M. Koppe, P. Denk, C. Waldauf, A. J. Heeger and C. J. Brabec, *Adv. Mater.*, 2006, **18**, 789.
16 L. J. A. Koster, V. D. Mihailetchi and P. W. M. Blom, *Appl. Phys. Lett.*, 2006, **88**, 093511.
17 G. Li, C. W. Chu, V. Shrotriya, J. Huang and Y. Yang, *Appl. Phys. Lett.*, 2006, **88**, 253503.
18 H. H. Liao, L. M. Chen, Z. Xu, G. Li and Y. Yang, *Appl. Phys. Lett.*, 2008, **92**, 173303.
19 Z. He, C. Zhong, S. Su, M. Xu, H. Wu and Y. Cao, *Nat. Photonics*, 2012, **6**, 591.
20 X. Guo, N. Zhou, S. J. Lou, J. Smith, D. B. Tice, J. W. Hennek, R. P. Ortiz, J. T. L. Navarrete, S. Li, J. Strzalka, L. X. Chen, R. P. H. Chang, A. Facchetti and T. J. Marks, *Nat. Photonics*, 2013, **7**, 825.
21 G. K. Mor, K. Shankar, M. Paulose, O. K. Varghese and C. A. Grimes, *Appl. Phys. Lett.*, 2007, **91**, 152111.
22 C. Waldauf, M. Morana, P. Denk, P. Schilinsky, K. Coakley, S. A. Choulis and C. J. Brabec, *Appl. Phys. Lett.*, 2006, **89**, 233517.
23 M. S. White, D. C. Olson, S. E. Shaheen, N. Kopidakis and D. S. Ginley, *Appl. Phys. Lett.*, 2006, **89**, 143517.
24 R. Steim, S. A. Choulis, P. Schilinsky and C. J. Brabec, *Appl. Phys. Lett.*, 2008, **92**, 093303.
25 T. Yang, W. Cai, D. Qin, E. Wang, L. Lan, X. Gong, J. Peng and Y. Cao, *J. Phys. Chem. C*, 2010, **114**, 6849.
26 H.-L. Yip and A. K.-Y. Jen, *Energy Environ. Sci.*, 2012, **5**, 5994.
27 S. Lee, B. Koo, J. Shin, E. Lee, H. Park and H. Kim, *Appl. Phys. Lett.*, 2006, **88**, 162109.
28 M. McDowell, I. G. Hill, J. E. McDermott, S. L. Bernasek and J. Schwartz, *Appl. Phys. Lett.*, 2006, **88**, 073505.
29 L. L. Chua, J. Zaumseil, J. F. Chang, E. C. W. Ou, P. K. H. Ho, H. Sirringhaus and R. H. Friend, *Nature*, 2005, **434**, 194.
30 Q. Wei, T. Nishizawa, K. Tajima and K. Hashimoto, *Adv. Mater.*, 2008, **20**, 2211.
31 Q. Mei, C. Li, X. Gong, H. Lu, E. Jin, C. Du, Z. Lu, L. Jiang, X. Meng, C. Wang and Z. Bo, *ACS Appl. Mater. Interfaces*, 2013, **5**, 8076.
32 C. Duan, W. Cai, B. B. Y. Hsu, C. Zhong, K. Zhang, C. Liu, Z. Hu, F. Huang, G. C. Bazan, A. J. Heeger and Y. Cao, *Energy Environ. Sci.*, 2013, **6**, 3022.
33 C. Duan, K. Zhang, C. Zhong, F. Huang and Y. Cao, *Chem. Soc. Rev.*, 2013, **42**, 9071.
34 H. Hoppe and N. S. Sariciftci, *J. Mater. Chem.*, 2006, **16**, 45 and references therein.
35 E. Klimov, W. Li, X. Yang, G. G. Hoffmann and J. Loos, *Macromolecules*, 2006, **39**, 4493.
36 Y.-C. Huang, S.-Y. Chuang, M.-C. Wu, H.-L. Chen, C.-W. Chen and W.-F. Su, *J. Appl. Phys.*, 2009, **106**, 034506.
37 H. Zhong, X. Yang, B. deWith and J. Loos, *Macromolecules*, 2006, **39**, 218.
38 X. Yang, J. K. J. van Duren, R. A. J. Janssen, M. A. J. Michels and J. Loos, *Macromolecules*, 2004, **37**, 2151.
39 A. Swinnen, I. Haeldermans, M. vande Ven, J. D'Haen, G. Vanhoyland, S. Aresu, M. D'Olieslaeger and J. Manca, *Adv. Funct. Mater.*, 2006, **16**, 760.
40 C. Muller, T. A. M. Ferenczi, M. Campoy-Quiles, J. M. Frost, D. D. C. Bradley, P. Smith, N. Stingelin-Stutzmann and J. Nelson, *Adv. Mater.*, 2008, **20**, 3510.
41 X. Yang, J. K. J. van Duren, M. T. Rispens, J. C. Hummelen, R. A. J. Janssen, M. A. J. Michels and J. Loos, *Adv. Mater.*, 2004, **16**, 802.
42 M. Jørgensen, K. Norrman and F. C. Krebs, *Sol. Energy Mater. Sol. Cells*, 2008, **92**, 686.
43 K. Sivula, C. K. Luscombe, B. C. Thompson and J. M. J. Fréchet, *J. Am. Chem. Soc.*, 2006, **128**, 13988.
44 Y. Zhang, H.-L. Yip, O. Acton, S. K. Hau, F. Huang and A. K. Y. Jen, *Chem. Mater.*, 2009, **21**, 2598.
45 C.-Z. Li, S.-C. Chien, H.-L. Yip, C.-C. Chueh, F.-C. Chen, Y. Matsuo, E. Nakamura and A. K. Y. Jen, *Chem. Commun.*, 2011, **47**, 10082.
46 F. B. Kooistra, J. Knol, F. Kastenberg, L. M. Popescu, W. J. H. Verhees, J. M. Kroon and J. C. Hummelen, *Org. Lett.*, 2007, **9**, 551.
47 C. Yang, J. Y. Kim, S. Cho, J. K. Lee, A. J. Heeger and F. Wudl, *J. Am. Chem. Soc.*, 2008, **130**, 6444.
48 M. Lenes, G.-J. A. H. Wetzelaer, F. B. Kooistra, S. C. Veenstra, J. C. Hummelen and P. W. M. Blom, *Adv. Mater.*, 2008, **20**, 2116.
49 Y. He, H.-Y. Chen, J. Hou and Y. Li, *J. Am. Chem. Soc.*, 2010, **132**, 1377.
50 Y.-J. Cheng, C.-H. Hsieh, Y. He, C.-S. Hsu and Y. Li, *J. Am. Chem. Soc.*, 2010, **132**, 17381.
51 G. Zhao, Y. He and Y. Li, *Adv. Mater.*, 2010, **22**, 4355.
52 Y. Li, *Chem. - Asian J.*, 2013, **8**, 2316.
53 Y. He, G. Zhao, B. Peng and Y. Li, *Adv. Funct. Mater.*, 2010, **20**, 3383.
54 Y. Sun, C. Cui, H. Wang and Y. Li, *Adv. Energy Mater.*, 2011, **1**, 1058.
55 X. Fan, C. Cui, C. Fang, J. Wang, S. Li, F. Cheng, H. Long and Y. Li, *Adv. Funct. Mater.*, 2012, **22**, 585.
56 X. Guo, C. Cui, M. Zhang, L. Huo, Y. Huang, J. Hou and Y. Li, *Energy Environ. Sci.*, 2012, **5**, 7943.
57 Y. He, B. Peng, G. Zhao, Y. Zou and Y. Li, *J. Phys. Chem. C*, 2011, **115**, 4340.
58 S.-H. Liao, Y.-L. Li, T.-H. Jen, Y.-S. Cheng and S.-A. Chen, *J. Am. Chem. Soc.*, 2012, **134**, 14271.
59 C. Zhang, S. Chen, Z. Xiao, Q. Zuo and L. Ding, *Org. Lett.*, 2012, **14**, 1508.

60 R. C. MacKenzie, I. J. M. Frost and J. Nelson, *J. Chem. Phys.*, 2010, **132**, 064904.
61 Y.-J. Cheng, M.-H. Liao, C.-Y. Chang, W.-S. Kao, C.-E. Wu and C.-S. Hsu, *Chem. Mater.*, 2011, **23**, 4056.
62 M. Eiermann, R. C. Haddon, B. Knight, Q. C. Li, M. Maggini, N. Martín, T. Ohno, M. Prato, T. Suzuki and F. Wudl, *Angew. Chem., Int. Ed. Engl.*, 1995, **34**, 1591.
63 Y.-J. Cheng, C.-H. Hsieh, P.-J. Li and C.-S. Hsu, *Adv. Funct. Mater.*, 2011, **21**, 1723.
64 A. Swinnen, I. Haeldermans, M. vande Ven, J. D'Haen, G. Vanhoyland, S. Aresu, M. D'Olieslaeger and J. Manca, *Adv. Funct. Mater.*, 2006, **16**, 760.
65 C. Müller, T. A. M. Ferenczi, M. Campoy-Quiles, J. M. Frost, D. D. C. Bradley, P. Smith, N. Stingelin-Stutzmann and J. Nelson, *Adv. Mater.*, 2008, **20**, 3510.
66 S. K. Hau, H.-L. Yip, O. Acton, N. S. Baek, H. Ma and A. K.-Y. Jen, *J. Mater. Chem.*, 2008, **18**, 5113.
67 S. K. Hau, H.-L. Yip, H. Ma and A. K.-Y. Jen, *Appl. Phys. Lett.*, 2008, **93**, 233304.
68 S. K. Hau, Y.-J. Cheng, H.-L. Yip, Y. Zhang, H. Ma and A. K.-Y. Jen, *ACS Appl. Mater. Interfaces*, 2010, **2**, 1892.
69 Y.-Y. Lai, P.-I. Shih, Y.-P. Li, C.-E. Tsai, J.-S. Wu, Y.-J. Cheng and C.-S. Hsu, *ACS Appl. Mater. Interfaces*, 2013, **5**, 5122.
70 C. Duan, C. Zhong, C. Liu, F. Huang and Y. Cao, *Chem. Mater.*, 2012, **24**, 1682.
71 C. M. Zhong, S. J. Liu, F. Huang, H. B. Wu and Y. Cao, *Chem. Mater.*, 2011, **23**, 4870.
72 C.-H. Hsieh, Y.-J. Cheng, P.-J. Li, C.-H. Chen, M. Dubosc, R.-M. Liang and C.-S. Hsu, *J. Am. Chem. Soc.*, 2010, **132**, 4887.
73 V. D. Mihailetchi, P. W. M. Blom, J. C. Hummelen and M. T. Rispens, *J. Appl. Phys.*, 2003, **94**, 6849.
74 P. W. M. Blom, V. D. Mihailetchi, L. J. A. Koster and D. E. Markov, *Adv. Mater.*, 2007, **19**, 1551.
75 M. T. Lloyd, D. C. Olson, P. Lu, E. Fang, D. L. Moore, M. S. White, M. O. Reese, D. S. Ginley and J. W. P. Hsu, *J. Mater. Chem.*, 2009, **19**, 7638.
76 M. O. Reese, M. S. White, G. Rumbles, D. S. Ginley and S. E. Shaheen, *Appl. Phys. Lett.*, 2008, **92**, 053307.
77 K. M. O'Malley, C.-Z. Li, H.-L. Yip and A. K.-Y. Jen, *Adv. Energy Mater.*, 2012, **2**, 82.
78 C.-Z. Li, C.-C. Chueh, H.-L. Yip, K. M. O'Malley, W.-C. Chen and A. K.-Y. Jen, *J. Mater. Chem.*, 2012, **22**, 8574.
79 A. A. Zakhidov, J.-K. Lee, H. H. Fong, J. A. DeFranco, M. Chatzichristidi, P. G. Taylor, C. K. Ober and G. G. Malliaras, *Adv. Mater.*, 2008, **20**, 3481.
80 S. Sax, N. Rugen-Penkalla, A. Neuhold, S. Schuh, E. Zojer, E. J. W. List and K. Müllen, *Adv. Mater.*, 2010, **22**, 2087.
81 Z.-G. Zhang, H. Li, Z. Qi, Z. Jin, G. Liu, J. Hou, Y. Li and J. Wang, *Appl. Phys. Lett.*, 2013, **102**, 143902.
82 J. Hou, H.-Y. Chen, S. Zhang, R. I. Chen, Y. Yang, Y. Wu and G. Li, *J. Am. Chem. Soc.*, 2009, **131**, 15586.
83 L. Huo, S. Zhang, X. Guo, F. Xu, Y. Li and J. Hou, *Angew. Chem., Int. Ed.*, 2011, **50**, 9697.
84 Z.-G. Zhang, H. Li, B. Qi, D. Chi, Z. Jin, Z. Qi, J. Hou, Y. Li and J. Wang, *J. Mater. Chem. A*, 2013, **1**, 9624.
85 C.-W. Liang, W.-F. Su and L. Wang, *Appl. Phys. Lett.*, 2009, **95**, 133303.
86 J.-S. Huang, C.-Y. Chou and C.-F. Lin, *Sol. Energy Mater. Sol. Cells*, 2010, **94**, 182.
87 Y.-J. Cheng, M. S. Liu, Y. Zhang, Y. Niu, F. Huang, J.-W. Ka, H.-L. Yip, Y. Tian and A. K.-Y. Jen, *Chem. Mater.*, 2008, **20**, 413.
88 F. Huang, Y.-J. Cheng, Y. Zhang, M. S. Liu and A. K.-Y. Jen, *J. Mater. Chem.*, 2008, **18**, 4495.
89 N. Cho, C.-Z. Li, H.-L. Yip and A. K.-Y. Jen, *Energy Environ. Sci.*, 2014, **7**, 638.
90 W. J. E. Beek, M. M. Wienk and R. A. J. Janssen, *Adv. Funct. Mater.*, 2006, **16**, 1112.
91 P. A. van Hal, M. P. T. Christiaans, M. M. Wienk, J. M. Kroon and R. A. J. Janssen, *J. Phys. Chem. B*, 1999, **103**, 4352.
92 Y.-H. Niu, M. S. Liu, J. W. Ka and A. K.-Y. Jen, *Appl. Phys. Lett.*, 2006, **88**, 093505.
93 R. Steim, S. A. Choulis, P. Schilinsky, U. Lemmer and C. J. Brabec, *Appl. Phys. Lett.*, 2009, **94**, 043304.
94 Z. Zhu, D. Waller, R. Gaudiana, M. Morana, D. Mühlbacher, M. Scharber and C. J. Brabec, *Macromolecules*, 2007, **40**, 1981.
95 C.-H. Chen, C.-H. Hsieh, M. Dubosc, Y.-J. Cheng and C.-S. Hsu, *Macromolecules*, 2010, **43**, 697.
96 M. D. McGehee, *MRS Bull.*, 2009, **34**, 95.
97 T. Sagawa, S. Yoshikawa and H. Imahori, *J. Phys. Chem. Lett.*, 2010, **1**, 1020.
98 C. Y. Kuo, W. C. Tang, C. Gau, T. F. Guo and D. Z. Jeng, *Appl. Phys. Lett.*, 2008, **93**, 033307.
99 J. S. Kim, Y. Park, D. Y. Lee, J. H. Lee, J. H. Park, J. K. Kim and K. Cho, *Adv. Funct. Mater.*, 2010, **20**, 540.
100 J. I. Lee, S. H. Cho, S. M. Park, J. K. Kim, J. W. Yu, Y. C. Kim and T. P. Russell, *Nano Lett.*, 2008, **8**, 2315.
101 J. Weickert, R. B. Dunbar, H. C. Hesse, W. Wiedemann and L. Schmidt-Mende, *Adv. Mater.*, 2011, **23**, 1810.
102 H. H. Wang, C. Y. Liu, S. B. Wu, N. W. Liu, C. Y. Peng, T. H. Chan, C. F. Hsu, J. K. Wang and Y. L. Wang, *Adv. Mater.*, 2006, **18**, 491.
103 N. W. Liu, C. Y. Liu, H. H. Wang, C. F. Hsu, M. Y. Lai, T. H. Chuang and Y. L. Wang, *Adv. Mater.*, 2008, **20**, 2547.
104 K. T. Tsai, Y. R. Huang, M. Y. Lai, C. Y. Liu, H. H. Wang, J. H. He and Y. L. Wang, *J. Nanosci. Nanotechnol.*, 2010, **10**, 8293.
105 C.-Y. Chang, C.-E. Wu, S.-Y. Chen, C. Cui, Y.-J. Cheng, C.-S. Hsu, Y.-L. Wang and Y. Li, *Angew. Chem., Int. Ed.*, 2011, **50**, 9386.
106 D. C. Müller, A. Falcou, N. Reckefuss, M. Rojahn, V. Wiederhirn, P. Rudati, H. Frohne, O. Nuyken, H. Becker and K. Meerholz, *Nature*, 2003, **421**, 829.
107 A. Santos, P. Formentín, J. Pallarés, J. Ferré-Borrull and L. F. Marsal, *Sol. Energy Mater. Sol. Cells*, 2010, **94**, 1247.
108 F. S. Kim, G. Ren and S. A. Jenekhe, *Chem. Mater.*, 2011, **23**, 682.
109 E. Bacher, M. Bayerl, P. Rudati, N. Reckefuss, C. D. Müller, K. Meerholz and O. Nuyken, *Macromolecules*, 2005, **38**, 1640.

110 M. C. Gather, A. Köhnen, A. Falcou, H. Becker and K. Meerholz, *Adv. Funct. Mater.*, 2007, **17**, 191.
111 P. Zacharias, M. C. Gather, M. Rojahn, O. Nuyken and K. Meerholz, *Angew. Chem., Int. Ed.*, 2007, **46**, 4388.
112 R. H. Goncalves, W. H. Schreiner and E. R. Leite, *Langmuir*, 2010, **26**, 11657.
113 Y.-J. Cheng, F.-Y. Cao, W.-C. Lin, C.-H. Chen and C.-H. Hsieh, *Chem. Mater.*, 2011, **23**, 1512.
114 A. Köhen, N. Riegel, J. H.-W. M. Kremer, H. Lademann, D. C. Müller and K. Meerholz, *Adv. Mater.*, 2009, **21**, 879.
115 V. N. Novikov and A. P. Sokolov, *Nature*, 2004, **431**, 961.
116 R. T. Weitz, U. Zschieschang, F. Effenberger, H. Klauk, M. Burghard and K. Kern, *Nano Lett.*, 2007, **7**, 22.
117 C. Kim, Z. Wang, H.-J. Choi, Y.-G. Ha, A. Facchetti and T. J. Marks, *J. Am. Chem. Soc.*, 2008, **130**, 6867.
118 Q. Huang, G. A. Evmenenko, P. Dutta, P. Lee, N. R. Armstrong and T. J. Marks, *J. Am. Chem. Soc.*, 2005, **127**, 10227.
119 R. P. Ortiz, A. Facchetti and T. J. Marks, *Chem. Rev.*, 2010, **110**, 205.
120 M. Shtein, J. Mapel, J. B. Benziger and S. R. Forrest, *Appl. Phys. Lett.*, 2002, **81**, 268.
121 H. Yan, B. J. Scott, Q. Huang and T. J. Marks, *Adv. Mater.*, 2004, **16**, 1948.
122 W.-W. Liang, C.-Y. Chang, Y.-Y. Lai, S.-W. Cheng, H.-H. Chang, Y.-Y. Lai, Y.-J. Cheng, C.-L. Wang and C.-S. Hsu, *Macromolecules*, 2013, **46**, 4781.
123 Y.-J. Cheng, S.-W. Cheng, C.-Y. Chang, W.-S. Kao, M.-H. Liao and C.-S. Hsu, *Chem. Commun.*, 2012, **48**, 3203.
124 S.-H. Liao, H.-J. Jhuo, Y.-S. Cheng and S.-A. Chen, *Adv. Mater.*, 2013, **25**, 4766.
125 Y. Liang, Z. Xu, J. Xia, S.-T. Tsai, Y. Wu, G. Li, C. Ray and L. Yu, *Adv. Mater.*, 2010, **22**, E135.
126 K. Sivula, Z. T. Ball, N. Watanabe and J. M. J. Fréchet, *Adv. Mater.*, 2006, **18**, 206.
127 C. Yang, J. K. Lee, A. J. Heeger and F. Wudl, *J. Mater. Chem.*, 2009, **19**, 5416.
128 Q. Tai, J. Li, Z. Liu, Z. Sun, X. Zhao and F. Yan, *J. Mater. Chem.*, 2011, **21**, 6848.
129 M.-H. Liao, C.-E. Tsai, Y.-Y. Lai, F.-Y. Cao, J.-S. Wu, Y.-C. Chen, C.-L. Wang, C.-S. Hsu, I. Liau and Y.-J. Cheng, *Adv. Funct. Mater.*, 2014, **24**, 1418.
130 Z. Li, H. C. Wong, Z. Huang, H. Zhong, C. H. Tan, W. C. Tsoi, J. S. Kim, J. R. Durrant and J. T. Cabral, *Nat. Commun.*, 2013, **4**, DOI: 10.1038/ncomms3227.
131 B. J. Kim, Y. Miyamoto, B. Ma and J. M. J. Fréchet, *Adv. Funct. Mater.*, 2009, **19**, 2273.
132 B. Gholamkhass and S. Holdcroft, *Chem. Mater.*, 2010, **22**, 5371.
133 Z. Zhu, S. Hadjikyriacou, D. Wallker and R. Gaudiana, *J. Macromol. Sci., Part A: Pure Appl. Chem.*, 2004, **41**, 1467.
134 M. Drees, H. Hoppe, C. Winder, H. Neugebauer, N. S. Sariciftci, W. Schwinger, F. Schäffler, C. Topf, M. C. Scharber, Z. Zhu and R. Gaudiana, *J. Mater. Chem.*, 2005, **15**, 5158.
135 J.-F. Nierengarten and S. Setayesh, *New J. Chem.*, 2006, **30**, 313.
136 R. S. Ruoff, D. S. Tse, R. Malhotra and D. C. Lorents, *J. Phys. Chem.*, 1993, **97**, 3379.
137 Y. Marcus, A. L. Smith, M. V. Korobov, A. L. Mirakyan, N. V. Avramenko and E. B. Stukalin, *J. Phys. Chem. B*, 2001, **105**, 2499.
138 C.-Z. Li, Y. Matsuo, T. Niinomi, Y. Sato and E. Nakamura, *Chem. Commun.*, 2010, **46**, 8582.
139 J.-S. Wu, Y.-Y. Lai, Y.-J. Cheng, C.-Y. Chang, C.-L. Wang and C.-S. Hsu, *Adv. Energy Mater.*, 2013, **3**, 457.
140 A. M. Rao, P. Zhou, K.-A. Wang, G. T. Hager, J. M. Holden, Y. Wang, W.-T. Lee, X.-X. Bi, P. C. Eklund, D. S. Cornett, M. A. Duncan and I. J. Amster, *Science*, 1993, **259**, 955.
141 DPP-TT-T is poly-thieno[3,2*b*] thiophene-diketopyrrolopyrrole-*co*-thiophene.